

1 *Connectome Harmonic Decomposition of Human Brain Dynamics Reveals a Landscape*
2 *of Consciousness*
3

4 Luppi A.I. ^{a,b,*}, Vohryzek J. ^{c,d}, Kringelbach M. L. ^{c,d}, Mediano P.A.M. ^e, Craig M. M. ^{a,b}, Adapa R. ^a,
5 Carhart-Harris, R. L. ^f, Roseman, L. ^f, Pappas I. ^{a,b,g}, Finoia P. ^{a,h}, Williams G. B. ^{b,i}, Allanson J. ^{b,j}, Pickard
6 J. D. ^{b,h,i}, Menon D. K. ^a, Atasoy S. ^{c,d}, & Stamatakis E.A. ^{a,b}

7
8 ^aDivision of Anaesthesia, School of Clinical Medicine, University of Cambridge, Cambridge, United Kingdom
9

10 ^bDepartment of Clinical Neurosciences, University of Cambridge, Cambridge, United Kingdom
11

12 ^cDepartment of Psychiatry, University of Oxford, Oxford, United Kingdom
13

14 ^dCenter for Music in the Brain, Aarhus University, Aarhus, Denmark
15

16 ^eDepartment of Psychology, University of Cambridge, Cambridge, United Kingdom
17

18 ^fCenter for Psychedelic Research, Department of Brain Sciences, Imperial College London, London, United
19 Kingdom
20

21 ^gDepartment of Psychology and Helen Wills Neuroscience Institute, University of California - Berkeley,
22 Berkeley, California, USA
23

24 ^hDivision of Neurosurgery, School of Clinical Medicine, University of Cambridge, Cambridge, United Kingdom
25

26 ⁱWolfson Brain Imaging Centre, University of Cambridge, Cambridge, United Kingdom
27

28 ^jDepartment of Neurosciences, Cambridge University Hospitals NHS Foundation, Addenbrooke's Hospital,
29 Cambridge, United Kingdom
30

31
32 *Corresponding author: email al857@cam.ac.uk

33

34 **ABSTRACT**
35

36 A central question in neuroscience is how cognition and consciousness arise from human
37 brain activity. Here, we decompose cortical dynamics of resting-state functional MRI into
38 their constituent elements: the harmonics of the human connectome. Mapping a wide
39 spectrum of consciousness onto these elementary brain states reveals a generalisable
40 connectome harmonic signature of loss of consciousness, whether due to anaesthesia or
41 severe brain injury. Remarkably, its mirror-reversed image corresponds to the harmonic
42 signature of the psychedelic state induced by ketamine or LSD, identifying meaningful

43 relationships between neurobiology, brain function, and conscious experience. The
44 repertoire of connectome harmonics further provides a fine-tuned indicator of level of
45 consciousness, sensitive to differences in anaesthetic dose and clinically relevant sub-
46 categories of patients with disorders of consciousness. Overall, we reveal that the
47 emergence of consciousness from human brain dynamics follows the same universal
48 principles shared by a multitude of physical and biological phenomena: the mathematics
49 of harmonic modes.

50
51

52 MAIN TEXT

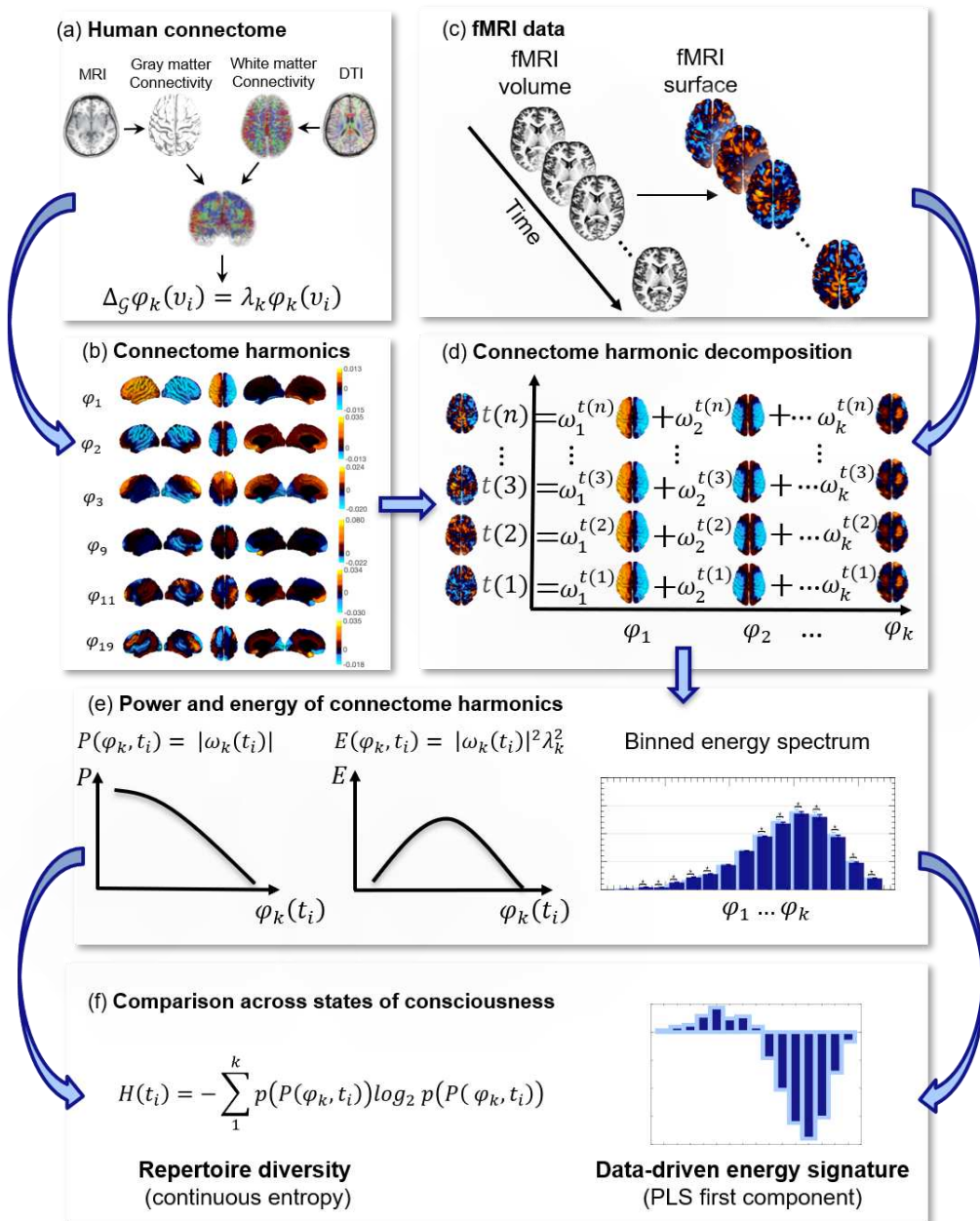
53
54 Relating subjective mental states to the underlying brain states remains a key challenge for
55 contemporary neuroscience¹. Despite recent advances, what remains elusive is a principled
56 account of how the spatio-temporal brain dynamics that support consciousness^{1–7}, arise
57 from the interplay of cortical dynamics across the brain’s anatomical connections⁸.

58
59 The emerging framework of connectome harmonic decomposition offers a way to bridge
60 this gap, decomposing complex brain dynamics (derived e.g. from functional MRI) in
61 terms of neurobiologically grounded, elementary brain states^{8–11}. Just like human language
62 can generate infinite meanings from recombination of a finite vocabulary, so the human
63 brain can generate an endless variety of mental states, by recombining a finite set of neural
64 building blocks. Mathematically, connectome harmonic decomposition (CHD) extends the
65 well-known Fourier transform to the human brain⁸. Through the Fourier transform, any
66 signal can be represented as a combination of fundamental sinusoids: the harmonic modes
67 of a linear filter. Likewise, CHD decomposes any pattern of cortical activity into a set of
68 universal basis functions of increasing spatial frequency (granularity): the harmonic modes
69 of the human connectome⁸. Harmonic modes are ubiquitous across natural phenomena,
70 ranging from acoustic vibrations and electron orbits, to animal coat patterns and

71 morphogenesis^{12,13}. In the human brain, harmonic modes (termed connectome harmonics;
72 though spherical harmonics have also been used¹⁴) emerge from the balance between
73 neuronal excitation and inhibition interacting over anatomical connections^{8,13}. Thus, CHD
74 provides an avenue to decompose and compare brain dynamics across states of
75 consciousness, in a way that is (i) universal across individuals, and (ii) grounded in brain
76 anatomy and neurophysiology⁸: a shared vocabulary for the language of human brain
77 activity, derived from fundamental mathematical principles. Here, we leverage the CHD
78 framework to map the landscape of human consciousness, revealing how connectome
79 harmonics orchestrate the emergence of different states of consciousness (Figure 1 and
80 Supplementary Figure 1).

81

82



83

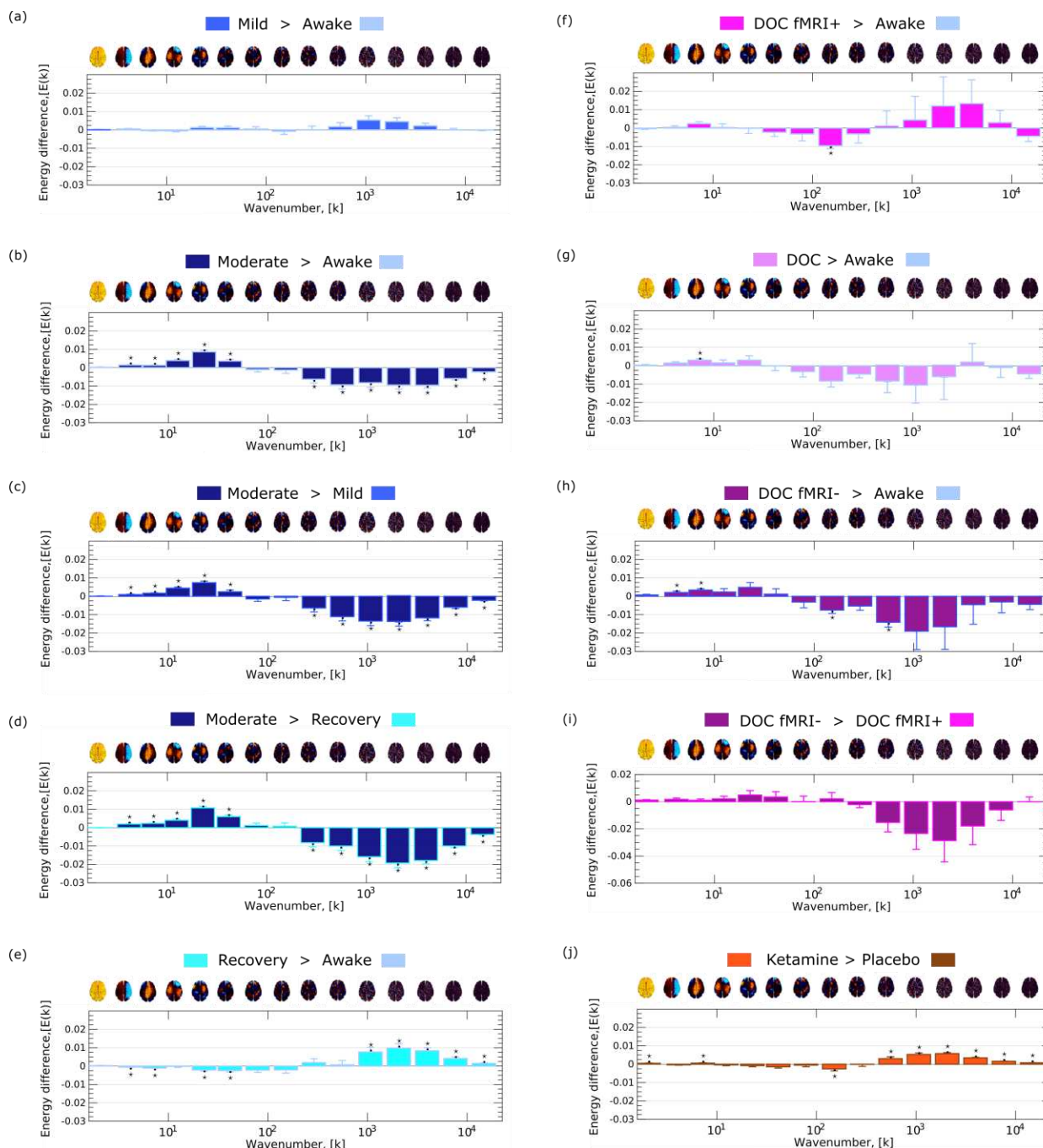
84

85 **Figure 1. Overview of connectome harmonics analysis framework.** (a) High-resolution rendering of
86 the human connectome is achieved by reconstructing the surface-based grey matter computed from
87 structural magnetic resonance imaging (sMRI) and the white-matter axonal tracts calculated with diffusion
88 tensor imaging (DTI). (b) Connectome harmonics are obtained as the eigenvectors of the graph Laplacian
89 applied to the human connectome. With an increasing connectome harmonic number k , we obtain more
90 complex and fine-grained spatial patterns. (c) Volumetric functional magnetic resonance imaging (fMRI)
91 data are projected onto the cortical surface for every timepoint t_i . (d) Connectome harmonic decomposition
92 (CHD) of the fMRI data estimates the contribution $\omega_k(t_i)$ of individual harmonics φ_k to the cortical
93 activity at every timepoint t_i . **Measures of the connectome harmonic spectrum.** (e) The power spectrum

94 is estimated as the absolute contribution $|\omega_k(t_i)|$ of individual harmonics φ_k to the fMRI data at every time
95 point t_i . Similarly, the energy spectrum is estimated as the square of the absolute contribution $|\omega_k(t_i)|$ of
96 individual harmonics φ_k to the fMRI data, weighted by the square of the harmonics'
97 corresponding eigenvalue λ_k at every time point t_i . The overall binned energy spectrum across subjects and
98 timepoints is constructed by discretising the energy of connectome harmonics in 15 logarithmically-spaced
99 frequency-specific bins, here shown for a target state (dark blue) and a reference state (light blue). (f)
100 Repertoire entropy is defined as the entropy of the power spectrum at every timepoint t_i , computed with the
101 continuous Kozachenko approximation; the data-driven energy signature of a target state of consciousness
102 is obtained from the first principal component of Partial Least Squares-Discriminant Analysis (PLS-DA),
103 which maximally discriminates the target state (dark blue) from the reference state (light blue), based on
104 their respective connectome harmonic energy spectra.
105

106 Connectome harmonic signatures of consciousness

107
108 Previous work has shown that CHD can identify consistent signatures of the psychedelic
109 state induced by the serotonin 5HT_{2A} receptor agonists LSD and psilocybin, in terms of a
110 shift in energy (normalised contribution) from low- to high-frequency harmonics,
111 corresponding to increasingly complex neural dynamics^{8–10}. The psychedelic state has
112 been postulated to represent one end of the spectrum of conscious states^{15,16}, with loss of
113 consciousness at the opposite end, in terms of subjective experience as well as observable
114 effects on brain function and dynamics^{7,17–21} (however, see Bayne and Carter (2018)²²). To
115 map the complete spectrum of consciousness, we therefore investigated resting-state
116 functional MRI (rs-fMRI) data from volunteers undergoing sedation with the intravenous
117 anaesthetic, propofol²³ (N=15). As an agonist of the chief inhibitory neurotransmitter
118 GABA, propofol enhances the activity of inhibitory interneurons, leading to globally
119 increased neuronal inhibition²⁴. Computational modelling has previously demonstrated
120 that a shift in energy from high- to low-frequency harmonics (i.e. the opposite of what is
121 observed with LSD and psilocybin^{8–10}) can arise from reduced global excitation or
122 increased global inhibition^{8,13}. Therefore, computational and theoretical reasons converge
123 to predict that propofol should induce connectome harmonic alterations that are the
124 opposite of what is observed with psychedelics.
125
126
127



128

129 **Figure 2. Frequency-specific energy changes across states of consciousness.** (a) Mild propofol sedation
130 > wakefulness. (b) Moderate anaesthesia > wakefulness. (c) Moderate anaesthesia > mild sedation.
131 (d) Moderate anaesthesia > post-anæsthetic recovery. (e) Recovery > wakefulness. (f) DOC patients > awake
132 healthy controls. (g) DOC fMRI+ patients > awake healthy controls. (h) DOC fMRI- patients > awake
133 healthy controls. (i) fMRI- > fMRI+ DOC patients. (j) Ketamine > placebo. * $p < 0.05$, FDR-corrected
134 across 15 frequency bins. A brain surface projection of the connectome harmonic pattern corresponding to
135 each frequency bin, averaged over the constituent spatial frequencies, is shown above each bin.

136

137

138 To further establish whether the connectome harmonic signature of anaesthesia is
139 representative of other ways of losing consciousness, we also considered a cohort of N=22
140 patients diagnosed with chronic disorders of consciousness arising from severe brain
141 injury³. We investigated whether CHD could detect consciousness in a subset of patients
142 who had previously exhibited evidence of covert consciousness by performing mental
143 imagery tasks in the scanner^{25,26} (in terms of specific brain regions activating when patients
144 were asked to imagine playing tennis or navigating around their house) (fMRI+; N=8),
145 compared with patients who had provided no such evidence (fMRI-; N=14).

146

147 Our results reveal a general connectome harmonic signature of loss of consciousness across
148 anaesthesia and disorders of consciousness (Figure 2, Supplementary Figure 2 and
149 Supplementary Table 1), characterised by a shift in the energy distribution from high to
150 low-frequency harmonic modes - the opposite of the pattern previously observed with
151 psychedelics^{9,10}. These characteristic alterations of connectome harmonic energy are
152 specific to loss of consciousness. Firstly, no significant energy alterations of the
153 connectome harmonic spectrum are observed during a lower dose of propofol
154 administration (mild sedation), when participants are still conscious. Instead, significant
155 alterations are only observed during moderate anaesthesia, once participants have lost
156 responsiveness. Secondly, the pattern observed during moderate anaesthesia is reversed
157 upon awakening. Thirdly, the same connectome harmonic signature is also observed for
158 chronic loss of consciousness induced by severe brain injury. A shift in energy from high
159 to low frequencies was found when comparing controls with unconscious (fMRI-) DOC
160 patients, with a similar trend also being evident when comparing the sub-groups of fMRI-
161 and fMRI+ (covertly conscious) DOC patients. Finally, this putative unconsciousness-
162 specific pattern of connectome harmonic energy was *not* observed when comparing fMRI+
163 DOC patients with awake volunteers – as we should expect from a specific marker of
164 unconsciousness, given that each fMRI+ patient had previously provided evidence of being
165 covertly conscious.

166

167 Intriguingly, the opposite pattern (elevated energy in high-frequency connectome
168 harmonics, and reduced energy in low-frequency ones) was observed when comparing
169 post-anaesthetic recovery and pre-anaesthetic wakefulness – resembling the pattern
170 previously observed with classic psychedelics^{9,10}. Extending the Wilson-Cowan neural
171 model to the human connectome, Atasoy and colleagues⁸ have previously demonstrated
172 that high-frequency harmonics emerge when excitation is increased, or inhibition is
173 diminished. Recovery from anaesthesia corresponds to a gradual reduction of the
174 (abnormally high) global inhibition induced by propofol. Thus, the resulting effects on the
175 energy distribution should be the same as those observed when increasing global excitation
176 (e.g. due to ketamine or LSD infusion), which is remarkably, precisely what we observed
177 here. Though speculative, this account may explain the well-known phenomenon whereby
178 individuals emerging from anaesthesia can exhibit symptoms of delirium, cognitive
179 alterations, and even hallucinations^{27,28}. Thus, our observed similarity between anaesthetic
180 emergence and psychedelics may provide a link between physiology (reduced neuronal
181 inhibition due to diminished levels of anaesthetic) and its corresponding cognitive
182 manifestation.

183
184 Having established that the connectome harmonic signature of loss of consciousness is the
185 same regardless of its cause, we investigated whether connectome harmonics could also
186 reveal a general signature of the psychedelic state. We reasoned that if the pattern of
187 connectome harmonic alterations induced by the serotonergic psychedelics LSD and
188 psilocybin^{9,10} represents a general signature of the psychedelic state, then the same
189 connectome harmonic signature should also be observed during psychedelic experiences
190 induced by drugs that operate through different molecular mechanisms. We investigated
191 this hypothesis with rs-fMRI data from N=20 volunteers undergoing infusion with a
192 psychoactive (sub-anaesthetic) dose of the N-methyl-D-aspartate receptor antagonist
193 ketamine^{29,30}, which induces dissociative symptoms and is considered to be a useful model
194 of psychosis^{29,31} (although see³²). Our results revealed an increase in the energy of high-
195 frequency harmonics, analogous to that induced by LSD and psilocybin^{9,10}.

196

197 The gradient from low- to high-frequency connectome harmonics reflects progressive
198 decoupling of the corresponding neural activity from the underlying structural
199 connectivity³³. Thus, the psychedelic-induced energy shift to high-frequency harmonics
200 indicates a departure from standard activity patterns encoded in the structural connectome,
201 in favour of increasingly diverse ones - a plausible neural correlate for the
202 phenomenologically rich state of mind induced by psychedelics⁸⁻¹⁰.

203

204

205 **Generalisability and predictive power of connectome harmonic signatures across states of**
206 **consciousness**

207

208 The emergence of two mirror-reversed patterns of connectome harmonic energy, one for
209 unconsciousness (whether due to anaesthesia or severe brain injury) and one for the
210 psychedelic state (whether induced by ketamine or serotonergic psychedelics^{9,10}), suggests
211 that it should be possible to generalise these patterns across datasets to establish the
212 harmonic signature of a) unconsciousness and b) psychedelic experience.

213

214 To pursue this hypothesis, we applied a data-driven technique known as Partial Least
215 Squares - Discriminant Analysis (PLS-DA)³⁴, to extract the multivariate pattern of
216 connectome harmonic energy that maximally distinguished between each pair of
217 conditions (termed multivariate signature, MVS; Supplementary Figure 3). We then
218 projected each subject's energy spectrum onto the MVS characterising a given state of
219 consciousness, to quantify their similarity (Methods). To investigate the generalisability of
220 the connectome harmonic signature of ketamine to other psychedelics, the LSD data
221 previously used by Atasoy and colleagues^{9,10} were also included in this new analysis.

222

223 Supporting the notion that two mirror-reversed patterns characterise loss of consciousness
224 and the psychedelic state, this analysis revealed similar projections for the multivariate

225 signatures (MVS) extracted from propofol anaesthesia (moderate vs awake) and from DOC
226 patients (fMRI- vs fMRI+), which were opposite of the projections onto ketamine (vs
227 placebo) and onto LSD (vs placebo) (Supplementary Figure 4 and Supplementary Table
228 2). The observation that loss of consciousness and the psychedelic state have diametrically
229 opposite harmonic signatures, also lends support for the intriguing possibility of employing
230 psychedelics to treat disorders of consciousness³⁵.

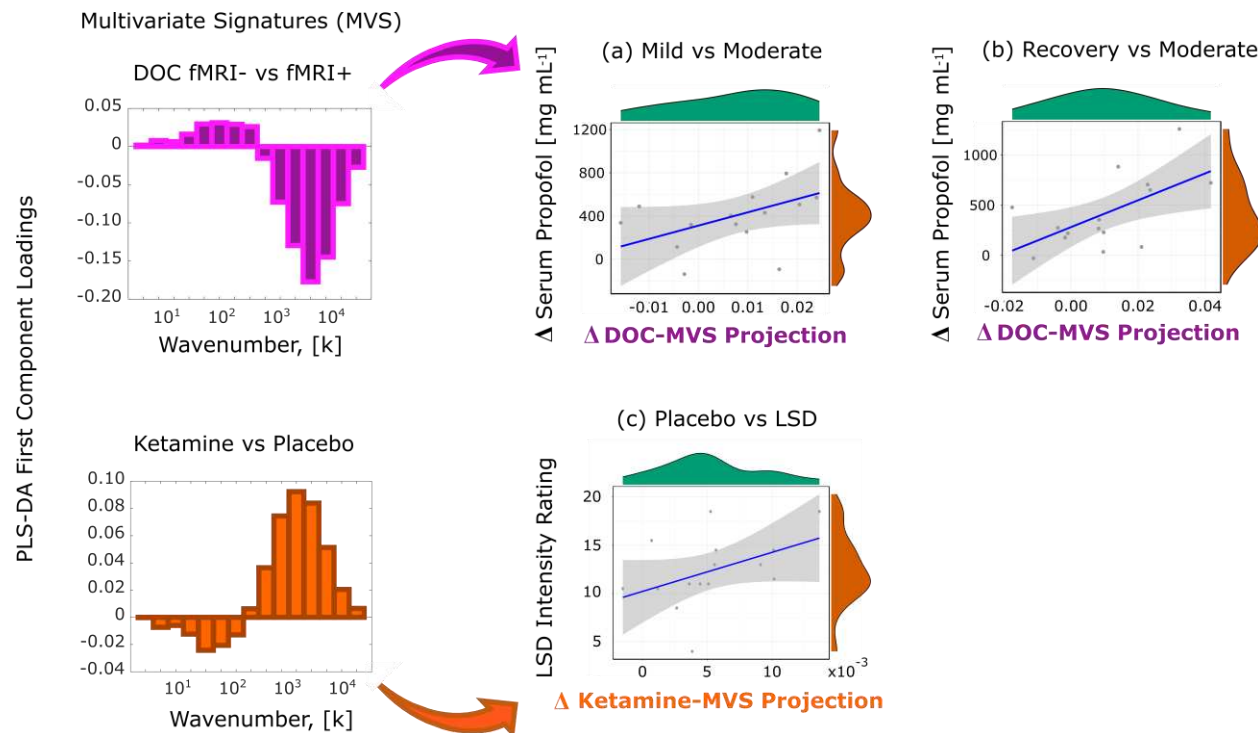
231

232 As an even more compelling demonstration that the signatures of unconsciousness
233 extracted from CHD are truly generalisable across ways of losing consciousness, we show
234 that individuals undergoing greater changes in propofol plasma concentration levels when
235 transitioning from consciousness to unconsciousness and back, also exhibit larger
236 differences in their correspondence to the harmonic pattern that discriminates between
237 covertly conscious and unconscious DOC patients.

238

239 Specifically, the propofol-induced change in fMRI projection score onto the multivariate
240 energy signature extracted from DOC patients, was significantly correlated with the change
241 in serum propofol levels when transitioning from mild to moderate propofol anaesthesia
242 (Spearman's $\rho = 0.57$, $CI_{95\%} [0.08, 0.84]$, $p = 0.026$; Figure 3a). Likewise, the change in
243 projection score onto the DOC MVS also predicted the change in serum propofol levels
244 between moderate sedation and post-anaesthetic recovery (Spearman's $\rho = 0.56$, $CI_{95\%}$
245 $[0.07, 0.83]$, $p = 0.030$; Figure 3b).

246



247

248 **Figure 3. Projection onto cross-dataset multivariate energy signatures (MVS) correlate with propofol**
249 **levels between consciousness and unconsciousness, and subjective intensity of the LSD experience.**
250 (a) Scatterplot of the change (moderate anaesthesia minus mild) in connectome harmonic energy projection
251 onto the multivariate energy signature (MVS) derived from the DOC dataset, versus the change in propofol
252 levels in volunteers' blood serum, between mild and moderate propofol anaesthesia. (b) Scatterplot of the
253 change (moderate minus recovery) in connectome harmonic energy projection onto the multivariate
254 signature derived from the DOC dataset, versus the change in propofol levels in volunteers' blood serum,
255 between moderate anaesthesia and recovery. (c) Scatterplot of the change (LSD minus placebo) in
256 connectome harmonic energy projection onto the multivariate signature derived from the ketamine dataset,
257 versus the subjective intensity of the psychedelic experience induced by LSD.

258

259

260 Furthermore, generalisability of connectome harmonic signatures also extends to the
261 psychedelic state: the subjective intensity of the psychedelic experience induced by LSD,
262 was predicted by the LSD-induced change in projection score onto the multivariate
263 signature derived from ketamine (Spearman's $\rho = 0.57$, $CI_{95\%} [0.08, 0.84]$, $p = 0.026$; Figure
264 3c). Importantly, the same MVS projections were not significantly correlated with
265 differences in subject motion, for both the propofol and LSD datasets, thereby excluding a
266 potential confound (Supplementary Table 3 and Supplementary Figure 5). These findings
267 identify general connectome harmonic signatures of conscious-to-unconscious transitions
268 (and vice a versa) induced by both propofol anaesthesia and DOC, as well as general

269 signatures of the psychedelic experience, relating neural dynamics to subjective
270 phenomenology.

271

272

273 **Repertoire diversity of connectome harmonics tracks level of consciousness**

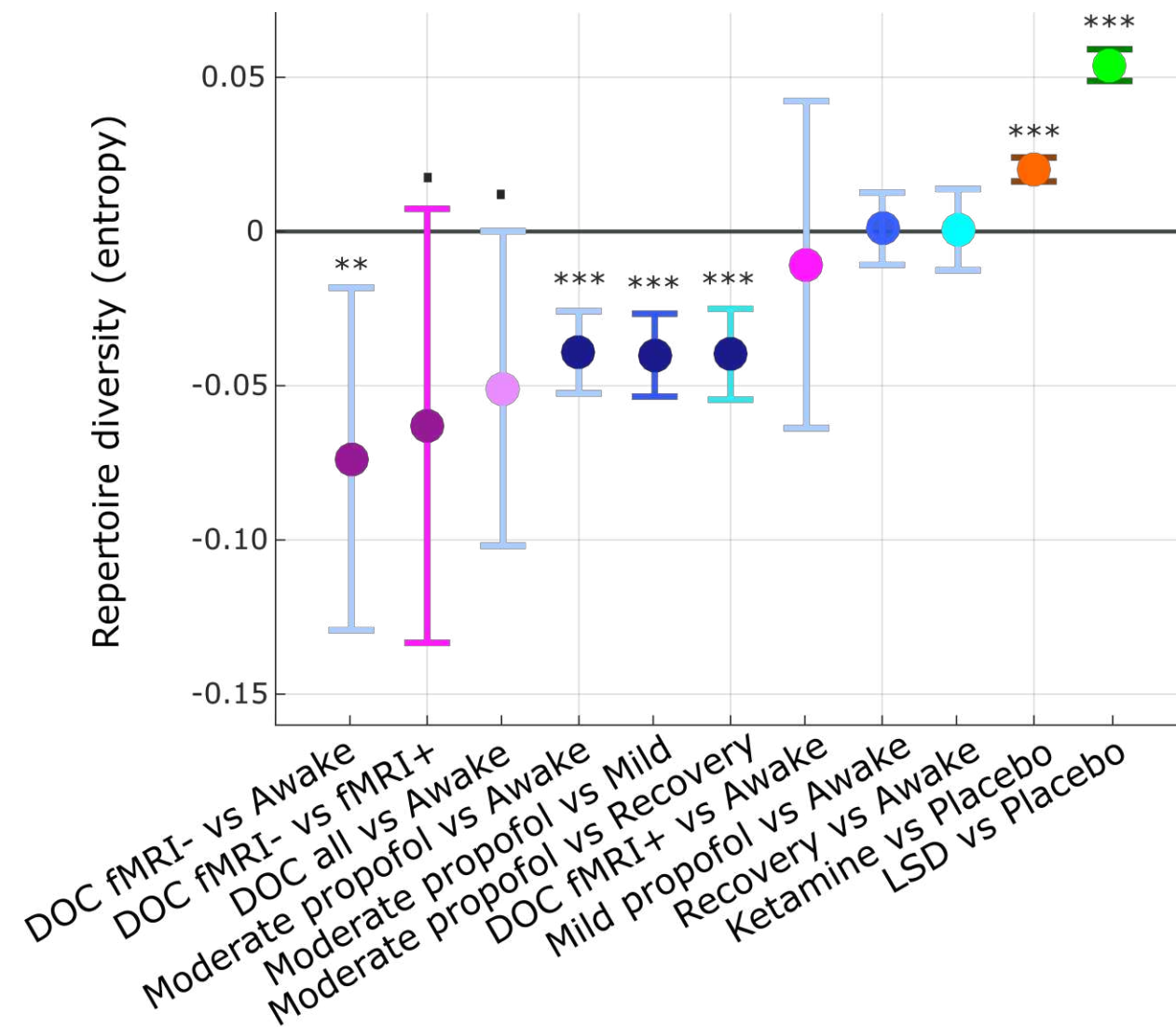
274

275 Finally, we investigated whether the diversity of mental experiences during a given state
276 of consciousness can be quantified in terms of diversity of connectome harmonic patterns
277 contributing to brain activity – the central tenet of recent theoretical efforts seeking to
278 establish a correspondence between the dynamics of mind and brain^{1,15}.

279

280 We therefore quantified the diversity of the distribution of harmonic power (absolute
281 magnitude of contribution) at each timepoint by means of the entropy of that distribution.
282 The higher the value of this measure, which we term “harmonic repertoire diversity”, the
283 wider the range of connectome harmonics that are recruited to compose cortical activity.
284 Thus, states of diminished consciousness, where the diversity of mental content is limited,
285 should be characterised by reduced entropy of the connectome harmonic repertoire,
286 reflecting a more restricted repertoire of brain patterns. Conversely, increased repertoire
287 diversity should be observed with ketamine and LSD, reflecting the high diversity of
288 experiences occurring in the psychedelic state^{15,16}.

289



290

291 **Figure 4. Diversity of connectome harmonic repertoire tracks level of consciousness from loss of**
292 **responsiveness to psychedelics.** Fixed effects (and 95% CI) of the comparison in repertoire diversity
293 (entropy of connectome harmonic power distribution) between pairs of conditions (states of consciousness),
294 treating condition as a fixed effect, and subjects as random effects. Timepoints were also included as
295 random effects, nested within subjects. *** $p < 0.001$; ** $p < 0.01$; . $p < 0.10$.

296

297 Our results support both of these predictions (Supplementary Table 4 and Figure 4).
298 Ketamine and LSD exhibited significantly higher diversity of the repertoire of connectome
299 harmonics than placebo, whereas moderate anaesthesia with propofol resulted in reduced
300 diversity when compared with wakefulness, recovery, and even mild sedation. Conversely,
301 neither of the latter conditions (during which volunteers were conscious) was significantly
302 different from normal wakefulness in terms of their diversity of harmonic repertoire,

303 despite the presence of propofol in the blood in both cases - thereby indicating that diversity
304 of the connectome harmonic repertoire tracks the level of consciousness rather than the
305 mere presence of propofol.

306

307 Remarkably, our analysis revealed that DOC patients who had previously exhibited
308 evidence of covert consciousness (fMRI+), also exhibited entropy levels approaching those
309 of awake volunteers – in sharp contrast with fMRI- patients, who had provided no evidence
310 of being conscious, and whose repertoire entropy was significantly compromised (Figure
311 4 and Supplementary Table 3). Thus, our results demonstrate that the diversity of
312 connectome harmonic repertoire (measured in terms of entropy) can track level of
313 consciousness on a one-dimensional scale.

314

315 Although our results pertaining to DOC patients consistently followed the same pattern as
316 moderate anaesthesia, they sometimes narrowly failed to reach statistical significance due
317 to the large variability among patients - which is hardly unexpected since DOC are highly
318 heterogeneous conditions, varying in the source, location and extent of brain damage.
319 Although these results warrant caution until replicated in a different dataset, none of our
320 conclusions rest solely on the results from the DOC dataset. We also acknowledge that loss
321 of behavioural responsiveness during anaesthesia may not always coincide with loss of
322 brain responsiveness and subjective experience³⁶⁻³⁸, and even failure to respond to the
323 fMRI mental imagery tasks cannot conclusively rule out residual consciousness in DOC
324 patients: future research may benefit from seeking convergence across different task-free
325 neural correlates of consciousness^{37,39,40}.

326

327 Nevertheless, it is noteworthy that although we stratified our DOC patients based on their
328 performance on mental imagery tasks in the scanner, our connectome harmonic analysis
329 was entirely based on resting-state (i.e., task-free) fMRI data, which imposes no cognitive
330 demands on patients, unlike task-based paradigms³⁹. Therefore, connectome harmonics
331 analysis of re-fMRI may represent a useful screening tool in the clinic to identify patients

332 who may be covertly conscious – contributing to alleviate the high rate of misdiagnoses
333 for DOC patients when relying solely on behavioural criteria³⁹, while demonstrating the
334 potential clinical value of CHD as a general neural marker of consciousness bypassing
335 overt behaviour.

336

337 [Connectome harmonics as a framework to characterise conscious states](#)

338

339 Across multiple datasets, we demonstrate that the emergence of consciousness from human
340 brain dynamics follows the same universal principles shared by a multitude of physical and
341 biological phenomena across scales: the mathematics of harmonic modes. Diversity of the
342 connectome harmonic repertoire can provide a useful one-dimensional indicator of level
343 of consciousness, sensitive to differences in anaesthetic dose (mild sedation vs moderate
344 anaesthesia vs recovery) as well as sub-categories of patients with disorders of
345 consciousness. Being grounded in the brain's anatomy and neurophysiology, connectome
346 harmonics provide a mathematically principled explanatory framework to understand the
347 loss of complexity that accompanies loss of consciousness. Namely, the collapse in the
348 connectome harmonic repertoire reported here may constitute the link between
349 neurobiology (propofol-induced global inhibition) and phenomenology (loss of subjective
350 experience, i.e. unconsciousness) by restricting the set of states available to the brain.

351

352 Yet, connectome harmonics offer a richer characterisation of conscious states that goes
353 beyond simple (though effective) complexity measures: the specific distribution of energy
354 over connectome harmonics may be used to characterise the quality of various states of
355 consciousness, in terms of being “unconscious-like” or “psychedelic-like” (or neither).
356 Indeed, our analyses uncovered that the connectome harmonic signature of post-anaesthetic
357 recovery (and, to a lesser extent, mild sedation), resembled the signature of the psychedelic
358 state – even though diversity of the repertoire was near baseline levels.

359

360 Thus, composition of the energy spectrum and diversity of the harmonic repertoire provide
361 distinct and synergistic insights to identify meaningful relationships between brain function
362 and conscious experience. Having demonstrated its power and generalisability across
363 datasets and states of consciousness, the framework of connectome harmonic
364 decomposition may be especially useful in the characterisation of a wider set of mental
365 states, from dreaming to psychosis.

366

367

368

369 MATERIALS AND METHODS

370

371 Ketamine Dataset

372

373 Recruitment

374 A total of 21 participants (10 males; mean age 28.7 years, SD = 3.2 years) were recruited via
375 advertisements placed throughout central Cambridge, UK. All participants underwent a screening
376 interview in which they were asked whether they had previously been diagnosed or treated for any
377 mental health problems and whether they had ever taken any psychotropic medications.
378 Participants reporting a personal history of any mental health problems or a history of any
379 treatment were excluded from the study. All participants were right-handed, were free of current
380 of previous psychiatric or neurological disorder or substance abuse problems, and had no history
381 of cardiovascular illness or family history of psychiatric disorder/substance abuse. The study was
382 approved by the Cambridge Local Research and Ethics Committee, and all participants provided
383 written informed consent in accordance with ethics committee guidelines. The acquisition and
384 design are described in detail in a previous study ²⁹.

385

386 Study Design

387 Participants were assessed on two occasions, separated by at least 1 week. On one occasion, they
388 received a continuous computer-controlled intravenous infusion of a racemic ketamine solution
389 (2 mg/ml) until a targeted plasma concentration of 100 ng/ml was reached. This concentration

390 was sustained throughout the protocol. A saline infusion was administered on the other occasion.
391 Infusion order was randomly counterbalanced across participants. The infusion was performed
392 and monitored by a trained anesthetist (RA) who was unblinded for safety reasons, but who
393 otherwise had minimal contact with participants. At all other times, participants were supervised
394 by investigators blinded to the infusion protocol. The participants remained blinded until both
395 assessments were completed. All MRI and assessment procedures were identical across
396 assessment occasions.

397

398 Infusion Protocol

399 Bilateral intravenous catheters were inserted into volunteers' forearms, one for infusion, and the
400 other for serial blood sampling. We used a validated and previously implemented ⁴¹ three-
401 compartment pharmacokinetic model to achieve a constant plasma concentration of 100 ng/ml
402 using a computerized pump (Graseby 3500, Graseby Medical, UK). The infusion continued for
403 15 min to allow stabilization of plasma levels. Blood samples were drawn before and after the
404 resting fMRI scan and then placed on ice. Plasma was obtained by centrifugation and stored at
405 -70 °C. Plasma ketamine concentrations were measured by gas chromatography-mass
406 spectrometry.

407

408 MRI Acquisition

409 Scanning was performed using a 3.0 T MRI scanner (Siemens Magnetom, Trio Tim, Erlangen,
410 Germany) equipped with a 12-channel array coil located at the Wolfson Brain Imaging Centre,
411 Addenbrooke's Hospital, Cambridge, UK. T2*-weighted echo-planar images were acquired under
412 eyes-closed resting-state conditions. Participants were instructed to close their eyes and let the
413 minds wander without going to sleep. Subsequent participant debriefing ensured that no
414 participants fell asleep during the scan. Imaging parameters were: 3x3x3.75mm voxel size, with a
415 time-to-repetition (TR) of 2000 ms, time-to-echo (TE) of 30 ms, flip angle of 78° in 64x64 matrix
416 size, and 240mm field of view (FOV). A total of 300 volumes comprising 32 slices each were
417 obtained. In addition, high- resolution anatomical T1 images were acquired using a three-
418 dimensional magnetic-prepared rapid gradient echo (MPPRAGE) sequence. In all, 176 contiguous
419 sagittal slices of 1.0mm thickness using a TR of 2300 ms, TE of 2.98 ms, flip angle of 91, and a
420 FOV of 256mm in 240x256 matrix were acquired with a voxel size of 1.0mm³. One participant
421 was excluded due to excessive movement, resulting in a final sample of N=20 subjects.

422

423 **Preprocessing**

424 We preprocessed the functional imaging data using a standard pipeline, implemented
425 within the SPM12-based (<http://www.fil.ion.ucl.ac.uk/spm>) toolbox CONN
426 (<http://www.nitrc.org/projects/conn>), version 17f ⁴². The pipeline comprised the
427 following steps: removal of the first five scans, to allow magnetisation to reach steady
428 state; functional realignment and motion correction; slice-timing correction to account for
429 differences in time of acquisition between slices; identification of outlier scans for
430 subsequent regression by means of the quality assurance/artifact rejection software *art*
431 (http://www.nitrc.org/projects/artifact_detect); spatial normalisation to Montreal
432 Neurological Institute (MNI-152) standard space with 2mm isotropic resampling
433 resolution, using the segmented grey matter image from each volunteer's high-resolution
434 T1-weighted image, together with an *a priori* grey matter template.

435

436 **Denoising**

437 To reduce noise due to cardiac and motion artifacts, we applied the anatomical CompCor method
438 of denoising the functional data ⁴³, also implemented within the CONN toolbox. The anatomical
439 CompCor method involves regressing out of the functional data the following confounding effects:
440 the first five principal components attributable to each individual's white matter signal, and the
441 first five components attributable to individual cerebrospinal fluid (CSF) signal; six subject-
442 specific realignment parameters (three translations and three rotations) as well as their first- order
443 temporal derivatives; the artifacts identified by *art*; and main effect of scanning condition⁴³. Linear
444 detrending was also applied, and the subject-specific denoised BOLD signal timeseries were band-
445 pass filtered to eliminate both low-frequency drift effects and high-frequency noise, thus retaining
446 temporal frequencies between 0.008 and 0.09 Hz. Importantly, note that this bandpass filtering
447 pertains to temporal frequencies, which are distinct from the spatial frequencies obtained from
448 connectome harmonic decomposition (as described below).

449

450

451 **Propofol Dataset**

452

453 Recruitment

454 Ethical approval for these studies was obtained from the Cambridgeshire 2 Regional Ethics
455 Committee, and all subjects gave informed consent to participate in the study. Sixteen healthy
456 volunteer subjects were recruited for scanning. The acquisition procedures are described in detail
457 in a previous study ²³. In addition to the original 16 volunteers, data were acquired for nine
458 additional participants using the same procedures, bringing the total number of participants in this
459 dataset to 25 (11 males, 14 females; mean age 34.7 years, SD = 9.0 years).

460

461 Propofol Infusion Protocol

462 The GABA-ergic intravenous agent propofol is one of the most commonly used anaesthetic drugs,
463 owing to the stability and predictability of its effects. Propofol was administered intravenously as
464 a “target controlled infusion” (plasma concentration mode), using an Alaris PK infusion pump
465 (Carefusion, Basingstoke, UK). Three target plasma levels were used - no drug (baseline), 0.6
466 mg/ml (mild sedation) and 1.2 mg/ml (moderate sedation).

467 A period of 10 min was allowed for equilibration of plasma and effect-site propofol concentrations.
468 Blood samples were drawn towards the end of each titration period and before the plasma target
469 was altered, to assess plasma propofol levels. In total, 6 blood samples were drawn during the
470 study. The mean (SD) measured plasma propofol concentration was 304.8 (141.1) ng/ml during
471 mild sedation, 723.3 (320.5) ng/ml during moderate sedation and 275.8 (75.42) ng/ml during
472 recovery. Mean (SD) total mass of propofol administered was 210.15 (33.17) mg, equivalent to
473 3.0 (0.47) mg/kg. The level of sedation was assessed verbally immediately before and after each
474 of the scanning runs. The three conditions from this dataset are referred to as Awake, Mild and
475 Moderate sedation respectively. Two senior anaesthetists were present during scanning sessions
476 and observed the subjects throughout the study from the MRI control room and on a video link
477 that showed the subject in the scanner. Electrocardiography and pulse oximetry were performed
478 continuously, and measurements of heart rate, non-invasive blood pressure, and oxygen saturation
479 were recorded at regular intervals.

480

481

482 **FMRI Data Acquisition**

483 The acquisition procedures are described in detail in the original study ²³. Briefly, MRI data were
484 acquired on a Siemens Trio 3T scanner (WBIC, Cambridge). Each functional BOLD volume
485 consisted of 32 interleaved, descending, oblique axial slices, 3 mm thick with interslice gap of 0.75
486 mm and in-plane resolution of 3 mm, field of view = 192x192 mm, repetition time = 2 s, acquisition
487 time = 2 s, time echo = 30 ms, and flip angle 78. We also acquired T1-weighted structural images
488 at 1 mm isotropic resolution in the sagittal plane, using an MPRAGE sequence with TR = 2250
489 ms, TI = 900 ms, TE = 2.99 ms and flip angle = 9 degrees, for localization purposes. Of the 25
490 healthy subjects, 15 were ultimately retained (7 males, 8 females): 10 were excluded, either
491 because of missing scans (n=2), or due to excessive motion in the scanner (n=8, 5mm maximum
492 motion threshold).

493

494 **Preprocessing and Denoising**

495 The same preprocessing and denoising procedures were followed as for the ketamine data.

496

497 **Disorders of Consciousness Patient Dataset**

498

499 **Recruitment**

500 A sample of 71 DOC patients was included in this study. Patients were referred from specialist
501 rehabilitation settings as well as specialist nursing homes specifically identified in the ethics. All
502 patients had been seen by a consultant neurologist or rehabilitation consultant before referral, to
503 make diagnosis as part of multidisciplinary assessments. To be included in the study, patients must
504 have had a DOC diagnosis, written informed consent to participation from their legal
505 representative as well as the consent of their treating physician, and they must be capable of being
506 transported to Addenbrooke's Hospital. The exclusion criteria included any medical condition that
507 made it unsafe for the patient to participate (decision made by clinical personnel blinded to the
508 specific aims of the study) or any reason they are unsuitable to enter the MRI scanner environment
509 (e.g. non-MRI-safe implants), significant pre-existing mental health problems, or insufficient
510 English pre injury. After admission to Addenbrooke's Hospital, each patient underwent clinical
511 neurological and neuroimaging testing, with pre-MRI CT for shunt management if needed.
512 Patients spent a total of five days (including arrival and departure days) at Addenbrooke's Hospital.

513 Coma Recovery Scale-Revised (CRS-R) assessments were recorded at least daily for the five days
514 of admission. If behaviours were indicative of awareness at any time, patients were classified as
515 MCS; otherwise UWS. We assigned MCS- or MCS+ sub-classification if behaviours were
516 consistent throughout the week. The most frequent signs of consciousness in MCS- patients are
517 visual fixation and pursuit, automatic motor reactions (e.g. scratching, pulling the bed sheet) and
518 localisation to noxious stimulation whereas MCS+ patients can, in addition, follow simple
519 commands, intelligibly verbalise or intentionally communicate^{44,45}. Scanning occurred at the
520 Wolfson Brain Imaging Centre, Addenbrooke's Hospital, between January 2010 and December
521 2015; medication prescribed to each patient was maintained during scanning. Ethical approval for
522 testing patients was provided by the National Research Ethics Service (National Health Service,
523 UK; LREC reference 99/391). All clinical investigations were conducted in accordance with the
524 Declaration of Helsinki.

525 As a focus of this study was on graph-theoretical properties of the brain, patients were
526 systematically excluded from the final cohort analysed in this study based on the following criteria:
527 1) large focal brain damage (i.e. more than 1/3 of one hemisphere) as stated by an expert in
528 neuroanatomy blinded to the patients' diagnoses; 2) excessive head motion during
529 resting state scanning (i.e. greater than 3mm in translation and/or 3 degrees in
530 rotation); 3) suboptimal segmentation and normalization of images. A total of 22 adults (14 males,
531 8 females; age range 17-70 years; mean time post injury: 13 months) meeting diagnostic criteria
532 for Unresponsive Wakefulness Syndrome/Vegetative State (N = 10) or Minimally Conscious State
533 (N = 12) due to brain injury were included in this study (Table 1).

534

535

536 Table 1: Demographic information for patients with Disorders of Consciousness.

Sex	Age	Months post injury	Aetiology	Diagnosis	CRS-R Score	Tennis	Spat Nav	Classification
M	46	23	TBI	UWS	6	no evidence	no evidence	fMRI-
M	57	14	TBI	MCS-	12	no evidence	no evidence	fMRI-
M	46	4	TBI	MCS	10	no evidence	no evidence	fMRI-
M	35	34	Anoxic	UWS	8	no evidence	no evidence	fMRI-
M	17	17	Anoxic	UWS	8	no evidence	positive	fMRI+
F	31	9	Anoxic	MCS-	10	no evidence	no evidence	fMRI-
F	38	13	TBI	MCS	11	positive	no evidence	fMRI+

M	29	68	TBI	MCS	10	SMA +ve	PPA +ve	fMRI+
M	23	4	TBI	MCS	7	SMA +ve	no evidence	fMRI+
F	70	11	Cerebral bleed	MCS	9	no evidence	no evidence	fMRI-
F	30	6	Anoxic	MCS-	9	PMC +ve	no evidence	fMRI+
F	36	6	Anoxic	UWS	8	no evidence	PPA +ve	fMRI+
M	22	5	Anoxic	UWS	7	no evidence	no evidence	fMRI-
M	40	14	Anoxic	UWS	7	no evidence	no evidence	fMRI-
F	62	7	Anoxic	UWS	7	no evidence	no evidence	fMRI-
M	46	10	Anoxic	UWS	5	no evidence	no evidence	fMRI-
M	21	7	TBI	MCS	11	no evidence	no evidence	fMRI-
M	67	14	TBI	MCS-	11	SMA +ve	PPA +ve	fMRI+
F	55	6	Hypoxia	UWS	12	negative	negative	fMRI-
M	28	14	TBI	MCS	8	positive	positive	fMRI+
M	22	12	TBI	MCS	10	negative	negative	fMRI-
F	28	8	ADEM	UWS	6	negative	negative	fMRI-

537 CRS-R, Coma Recovery Scale-Revised; UWS, Unresponsive Wakefulness Syndrome; MCS, Minimally Conscious
538 State; TBI, Traumatic Brain Injury; fMRI-, negative responders to mental imagery task; fMRI+, positive responders
539 to mental imagery task; SMA, supplementary motor area; PPA, parahippocampal place area; PMC, pre-motor cortex.
540

541

542 Stratification of DOC Patients into fMRI+ and fMRI-

543 Patients were stratified into two groups based on their ability to perform volitional tasks (mental
544 imagery) in the scanner. The mental imagery tasks used here have been previously used to assess
545 the presence of covert consciousness in DOC patients ^{25,26} and their validity has been confirmed
546 in healthy individuals ⁴⁶.

547

548 Patients were instructed to perform two mental imagery tasks. The first task involved motor
549 imagery (“tennis task”): each patient was asked to imagine being on a tennis court swinging their
550 arm to hit the ball back and forth with an imagined opponent. The second was a task of spatial
551 imagery (“navigation task”): the patient was required to imagine walking around the rooms of their
552 house, or the streets of a familiar city, and to visualise what they would see if they were there.
553 Each task comprised five cycles of alternating imagery and rest blocks, each lasting 30 seconds.
554 The two kinds of mental imagery blocks were cued with the spoken word “tennis” or “navigation”,
555 respectively, whereas the resting blocks were cued with the word “relax”, corresponding to
556 instructions for the patient to just stay still and keep their eyes closed.

557

558 Univariate fMRI analysis was conducted on all 22 patients for both the motor and spatial mental
559 imagery tasks. The analyses were performed using FSL version 5.0.9
560 (<https://fsl.fmrib.ox.ac.uk/fsl/fslwiki/>). The results of these analyses determined which patients
561 would be placed in each classification condition. For each functional scan, a general linear model
562 consisting of contrasting periods of rest and active imagery was computed. Results were
563 considered significant at a cluster level of $z > 2.3$ (corrected $p < 0.05$)²⁶.

564

565 Patients who exhibited significantly greater brain activation during either of the volitional mental
566 imagery tasks than rest (i.e. those who exhibited evidence of being able to respond to the task)
567 were deemed to be covertly conscious ($N = 8$); for brevity, we refer to these positive responders
568 as “fMRI+”. Conversely, we refer to patients who did not respond to either task (negative
569 responders), and who therefore did not exhibit detectable evidence of covert consciousness ($N =$
570 14), as “fMRI-”. (Table 1).

571

572 Resting-state FMRI Data Acquisition

573 Resting-state fMRI was acquired for 10 minutes (300 volumes, TR=2000ms) using a Siemens Trio
574 3T scanner (Erlangen, Germany). Functional images (32 slices) were acquired using an echo planar
575 sequence, with the following parameters: 3 x 3 x 3.75mm resolution, TR = 2000ms, TE = 30ms,
576 78 degrees FA. Anatomical scanning was also performed, acquiring high-resolution T1-weighted
577 images with an MPRAGE sequence, using the following parameters: TR = 2300ms, TE = 2.47ms,
578 150 slices, resolution 1 x 1 x 1mm.

579

580 rsfMRI Preprocessing and Denoising

581 Due to the presence of deformations caused by brain injury, rather than relying on automated
582 pipelines, patients’ brains were individually preprocessed using SPM12, with visual inspections
583 after each step. Additionally, to further reduce potential movement artifacts, data underwent
584 despiking with a hyperbolic tangent squashing function. The remaining preprocessing and
585 denoising steps were the same as described above for the ketamine and propofol data.

586

587 LSD Dataset

588

589 Recruitment

590 This study was approved by the National Research Ethics Service Committee London–West
591 London and was conducted in accordance with the revised declaration of Helsinki (2000), the
592 International Committee on Harmonization Good Clinical Practice guidelines and National Health
593 Service Research Governance Framework. Imperial College London sponsored the research,
594 which was conducted under a Home Office license for research with schedule 1 drugs.

595

596 All participants were recruited via word of mouth and provided written informed consent to
597 participate after study briefing and screening for physical and mental health. The screening for
598 physical health included electrocardiogram (ECG), routine blood tests, and urine test for recent
599 drug use and pregnancy. A psychiatric interview was conducted and participants provided full
600 disclosure of their drug use history. Key exclusion criteria included: < 21 years of age, personal
601 history of diagnosed psychiatric illness, immediate family history of a psychotic disorder, an
602 absence of previous experience with a classic psychedelic drug (e.g. LSD, mescaline,
603 psilocybin/magic mushrooms or DMT/ayahuasca), any psychedelic drug use within 6 weeks of the
604 first scanning day, pregnancy, problematic alcohol use (i.e. > 40 units consumed per week), or a
605 medically significant condition rendering the volunteer unsuitable for the study.

606

607 LSD Infusion Protocol

608 The data acquisition protocols were described in detail in a previous paper ⁴⁷, so we will describe
609 them in brief here. Twenty healthy volunteers with a previous experience using psychedelic drugs
610 were scanned. Patients underwent two scans, 14 days apart. On one day they were given a placebo
611 (10-mL saline) and the other they were given an active dose of LSD (75 µg of LSD in 10-mL
612 saline). The infusion (drug/placebo) was administered over 2 min and occurred 115min before the
613 resting-state scans were initiated. After infusion, subjects had a brief acclimation period in a mock
614 MRI scanner to prepare them for the experience of being in the real machine. ASL and BOLD
615 scanning consisted of three seven-minute eyes closed resting state scans.

616

617 FMRI Data Acquisition

618 The first and third scans were eyes-closed, resting state without stimulation, while the

619 second scan involved listening to music; however, this scan was not used in this analysis. The
620 precise length of each of the two BOLD scans included here was 7:20 minutes. Imaging was
621 performed on a 3T GE HDx system. High-resolution anatomical images were acquired with 3D
622 fast spoiled gradient echo scans in an axial orientation, with field of view = 256x256x192 and
623 matrix = 256x256x129 to yield 1mm isotropic voxel resolution. TR/TE = 7.9/3.0ms; inversion
624 time = 450ms; flip angle = 20.

625

626 BOLD-weighted fMRI data were acquired using a gradient echo planer imaging sequence, TR/TE
627 = 2000/35ms, FoV = 220mm, 64x64 acquisition matrix, parallel acceleration factor = 2, 90 flip
628 angle. Thirty five oblique axial slices were acquired in an interleaved fashion, each 3.4mm thick
629 with zero slice gap (3.4mm isotropic voxels). One subject aborted the experiment due to anxiety
630 and four others were excluded for excessive motion (measured in terms of frame-wise displacement),
631 leaving 15 subjects for analysis (11 males, 4 females; mean age 30.5 years, SD = 8.0 years)⁴⁷.

632

633 Preprocessing and Denoising

634 The same preprocessing and denoising procedures were followed as for the previous
635 datasets.

636

637

638 Connectome Harmonic Decomposition

639

640 Theoretical background

641 The core technique employed here relies on the recently developed framework of connectome
642 harmonic decomposition (CHD)^{9,13}. This technique allows patterns of brain activity derived from
643 functional MRI over time to be decomposed into a linear combination of a finite number of
644 orthogonal, synchronous brain states, the harmonic modes of the human structural connectome
645 (i.e. the network of anatomical connections between brain regions).

646

647 Each of these elementary brain states, also referred to as a connectome harmonics, is a pattern of
648 synchronised cortical activity associated with a specific spatial frequency (i.e. granularity),
649 corresponding to an intrinsic spatial wavenumber, k . Connectome harmonic decomposition may

650 therefore be seen as an extension of the well-known Fourier transform to the human connectome,
651 since the Fourier transform is a special case of harmonic mode decomposition applied to a 1D
652 domain with cyclic boundary conditions. Crucially, however, it is important to note that the
653 frequencies associated with each connectome harmonic are in the spatial rather than temporal
654 domain, and should not be confused with the frequencies identified by Fourier transform in the
655 temporal domain (e.g. for denoising of timeseries).

656

657 Construction of structural connectome

658 In order to identify the harmonic modes of the human structural connectome, which form the basis
659 function for our connectome harmonic decomposition of functional MRI data, we began by
660 constructing a network of anatomical connectivity between brain regions. To this end, we used
661 DTI and MRI data from an independent sample of 10 subjects from the Human Connectome
662 Project (HCP; Principal Investigators: David Van Essen and Kamil Ugurbil; 1U54MH091657,
663 funded by the 16 NIH Institutes and Centers that support the NIH Blueprint for Neuroscience
664 Research and by the McDonnell Center for Systems Neuroscience at Washington University;
665 <https://db.humanconnectome.org>). The workflow was the same as described in previous work by
666 Atasoy and colleagues ^{9,13}.

667

668 Freesurfer (<http://freesurfer.net>) was used to reconstruct the cortical surfaces at the interface of
669 white and grey matter based on the 0.7-mm resolution data from T1-weighted MRI. This resulted
670 in a network representation of 20,484 nodes (10,242 nodes per hemisphere) for each subject.
671 Subsequently, deterministic tractography was used to reconstruct cortico-cortical and thalamo-
672 cortical white matter fibres. After coregistering each subject's DTI and cortical surface data, each
673 of the 20,484 nodes of the reconstructed cortical surface network was used as a centre to initialise
674 eight seeds for deterministic tractography, implemented with the MrDiffusion tool
675 (<http://white.stanford.edu/newlm/index.php/MrDiffusion>). Tracking was terminated when
676 fractional anisotropy (FA) was below a threshold of 0.3, with 20mm minimum tract length, and
677 setting 30 degrees as the maximum allowed angle between consecutive tracking steps.

678

679 Extraction of connectome harmonics

680 The structural connectome of each subject was represented as a binary adjacency matrix A , such
681 that for each pair i and j of the $n = 20,484$ surface grey matter nodes, A_{ij} was set to 1 if a white
682 matter tract existed connecting them or if they were adjacent in the gray matter cortical surface
683 representation, and 0 otherwise, thereby yielding a symmetric (undirected) binary matrix¹³. The
684 individual adjacency matrices were then averaged across the 10 subjects to obtain a group average
685 matrix \bar{A} . We then define the degree matrix D of the graph as:

$$686 D(i, i) = \sum_{j=1}^n \bar{A}(i, j).$$

(1)

687 Following^{13,48}, we compute the symmetric graph Laplacian Δ_G on the group-average adjacency
688 matrix \bar{A} that represents the human connectome, in order to estimate the connectome Laplacian
689 (discrete counterpart of the Laplace operator Δ ⁴⁸ applied to the network of human structural brain
690 connectivity):

$$692 \Delta_G = D^{-1/2} L D^{-1/2}, \text{with } L = D - \bar{A}.$$

(2)

694

695 We then calculate the connectome harmonics φ_k , $k \in \{1, \dots, 18,715\}$ by solving the following
696 eigenvalue problem:

$$697 \Delta_G \varphi_k(v_i) = \lambda_k \varphi_k(v_i) \quad \forall v_i \in V, \quad \text{with } 0 < \lambda_1 < \lambda_2 < \dots < \lambda_n,$$

(3)

699

700 where λ_k , $k \in \{1, \dots, n\}$ is the corresponding eigenvalue of the eigenfunction φ_k , V is the set of
701 cortical surface vertices and n represents the number of vertices. In other words, λ_k and φ_k are the
702 eigenvalues and eigenvectors of the Laplacian of the human structural connectivity network,
703 respectively. Therefore, if φ_k is the connectome harmonic pattern of the k^{th} spatial frequency, then
704 the corresponding eigenvalue λ_k is a term relating to the intrinsic energy of the that particular
705 harmonic mode.

706

707 Connectome-harmonic decomposition of fMRI data.

708 At each timepoint $t \in \{1, \dots, T\}$ (corresponding to one TR), the fMRI data were projected onto
709 cortical surface coordinates by means of the Human Connectome Project Workbench -volume-to-

710 *surface-mapping* tool. Then, the spatial pattern of cortical activity over vertices v at time t , denoted
711 as $F_t(v)$, was decomposed as a linear combination of the set of connectome harmonics $\Psi =$
712 $\{\varphi_k\}_{k=1}^N$:

713

$$714 \quad F_t = \omega_1(t)\varphi_1 + \omega_2(t)\varphi_2 + \dots + \omega_n(t)\varphi_n = \sum_{k=1}^n \omega_k(t)\varphi_k(v) \quad (4)$$

715 with the contribution $\omega_k(t)$ of each connectome harmonic φ_k at time t being estimated as the
716 projection (dot product) of the fMRI data $F_t(v)$ onto φ_k :

717

$$719 \quad \omega_k(t) = \langle F_t, \varphi_k \rangle. \quad (5)$$

720

721

722 Power and Energy of connectome harmonics

723 Once the fMRI cortical activation pattern at time t has been decomposed into a linear combination
724 of connectome harmonics, the magnitude of contribution to cortical activity of each harmonic φ_k ,
725 $k \in \{1, \dots, n\}$ (regardless of sign) at any given timepoint t ($P(\varphi_k, t)$), called its “power” for
726 analogy with the Fourier transform, is computed as the amplitude of its contribution:

727

$$728 \quad P(\varphi_k, t) = |\omega_k(t)|. \quad (6)$$

729

730

731 In turn, the normalized frequency-specific contribution of each harmonic φ_k , $k \in \{1, \dots, n\}$ at
732 timepoint t , termed “energy”, is estimated by combining the strength of activation (power) of a
733 particular connectome harmonic with its own intrinsic energy given by λ_k^2 :

734

$$735 \quad E(\varphi_k, t) = |\omega_k(t)|^2 \lambda_k^2. \quad (7)$$

736

737 Consequently, total brain energy at time t is given by

738

739
$$E_{total}(t) = \sum_{k=1}^n |\omega_k(t)|^2 \lambda_k^2 = \|\Delta F_t(v)\|^2. \quad (8)$$

740
741
742 Since the Laplace operator Δ represents the amount of activity flow, the latter part of Equation 8
743 indicates that the total brain energy at a given point in time can be interpreted as the total cortical
744 flow of neural activity at that time⁹.

745
746

747 **Data-driven extraction of multivariate energy signatures**

748
749 Partial least squares (PLS, also known as Projection on Latent Spaces) is a multivariate statistical
750 analysis used to identify relationships between sets of variables X (predictors) and Y (targets), in
751 order to extract principal components as linear combinations of variables in each set that
752 maximally covary with each other³⁴. In the present case, for each pair of states of consciousness
753 under comparison, X was the matrix of 15 binned energy values per subject (averaged over
754 timepoints), and Y was the vector of binary classification between the two states (here, target vs
755 baseline state of consciousness, e.g. anaesthetised vs awake, ketamine vs placebo, fMRI- vs fMRI+
756 DOC, etc) – making this an application of Partial Least Squares Discriminant Analysis (PLS-DA),
757 owing to the binary nature of Y⁴⁹.

758
759 The first principal component extracted by PLS-DA represents the single most discriminative
760 pattern present in the data, in terms of distinguishing observations (subjects) belonging to the two
761 different classes (states of consciousness). Here, we refer to this pattern as the “multivariate
762 signature” (MVS).

763
764 To determine the cross-dataset generalisability of multivariate signatures, we selected four source
765 MVSs: one from the contrast between awake and moderate propofol anaesthesia; one from the
766 contrast between fMRI+ and fMRI- DOC patients; one from the contrast between placebo and
767 ketamine; and one from the contrast between placebo and LSD. For each subject and condition,
768 each source MVS was projected onto the pattern of binned connectome harmonic energy at each
769 timepoint, by taking their dot product. The result is a measure of the match between the relevant

770 multivariate signature and the harmonic energy, for each timepoint of each subject, which can then
771 be compared across states of consciousness.

772

773

774 Diversity of connectome harmonic repertoire

775

776 To quantify the diversity of the repertoire of connectome harmonics recruited at each point in time,
777 we start by observing that a diverse repertoire is one in which different harmonic modes contribute
778 in different degrees to brain activity – neither one single mode dominating (which would
779 correspond to a periodic oscillation) nor every mode contributing the same as every other mode
780 (which would correspond to white noise). To capture this
781 intuition, we quantify repertoire diversity in terms of the entropy of the distribution of connectome
782 harmonic power (absolute strength of contribution to the cortical activation pattern) at each
783 timepoint, which we calculate for each timepoint of each subject.

784

785 Specifically, to deal with continuous data (as in the present case) we rely on the Kozachenko
786 approximation, as implemented in the Java Information Dynamics Toolbox (JIDT;
787 <http://jlizier.github.io/jidt/>)⁵⁰. We note that when dealing with continuous variables, entropy can
788 have negative values⁵¹, but its interpretation remains the same: a more entropic distribution (i.e.
789 having a value of entropy closer to positive infinity) will correspond to a more diverse repertoire.

790

791 Statistical Analysis

792

793 Linear Mixed Effects models (implemented as the MATLAB function *fitlme*) were used to assess
794 the statistical significance of the differences between conditions (states of consciousness), treating
795 condition as a fixed effect, and subjects as random effects. When one measurement was obtained
796 for each timepoint, timepoints were also included as random effects, nested within subjects.
797 Results are reported in terms of the fixed effect of condition, and the upper and lower bounds of
798 its 95% confidence interval, with associated p-value. For comparison of frequency-specific
799 harmonic energy, the False Discovery Rate for multiple comparisons across 15 frequency bins was
800 controlled by means of the Benjamini-Hochberg procedure⁵².

801
802

803 [Acknowledgements](#)

804
805 AIL, JV and PAMM would like to thank Lena Dorfschmidt for co-organising OxBridge BrainHack
806 2019, where this work began. We also thank all volunteers and patients who provided data.
807 **Funding:** This work was supported by grants from the UK Medical Research Council
808 (U.1055.01.002.00001.01) [JDP]; The James S. McDonnell Foundation [JDP]; The Canadian
809 Institute for Advanced research (CIFAR) [DKM and EAS]; The National Institute for Health
810 Research (NIHR, UK), Cambridge Biomedical Research Centre and NIHR Senior Investigator
811 Awards [JDP and DKM]; The British Oxygen Professorship of the Royal College of Anaesthetists
812 [DKM]; The Stephen Erskine Fellowship, Queens' College, University of Cambridge [EAS]; The
813 Evelyn Trust, Cambridge and the EoE CLAHRC fellowship [JA]; The Gates Cambridge Trust
814 [AIL]; The Cambridge International Trust and the Howard Sidney Sussex Studentship [MMC];
815 The Oon Khye Beng Ch'Hia Tsio Studentship for Research in Preventive Medicine, Downing
816 College, University of Cambridge [IP]; The Wellcome Trust (grant no. 210920/Z/18/Z) [PAMM];
817 The European Research Council Consolidator Grant CAREGIVING (615539) [MLK and SA];
818 The Center for Music in the Brain, funded by the Danish National Research Foundation
819 (DNRF117) [MLK, SA and JV]; The Centre for Eudaimonia and Human Flourishing, funded by
820 the Pettit and Carlsberg Foundations [MLK]; The Imperial College President's Scholarship [LR];
821 The Alex Mosley Charitable Trust [RLCH]; The Wellcome Trust Research Training Fellowship
822 (grant no. 083660/Z/07/Z), Raymond and Beverly Sackler Studentship, and the Cambridge
823 Commonwealth Trust [RA]. The ketamine study was funded by the Bernard Wolfe Health
824 Neuroscience Fund and the Wellcome Trust. The original LSD study received support from a
825 Crowd Funding Campaign and the Beckley Foundation, as part of the Beckley-Imperial Research
826 Programme. The research was also supported by the NIHR Brain Injury Healthcare Technology
827 Co-operative based at Cambridge University Hospitals NHS Foundation Trust and University of
828 Cambridge. Data used to obtain the human connectome were provided by the Human Connectome
829 Project, WU-Minn Consortium (Principal Investigators: David Van Essen and Kamil Ugurbil;
830 1U54MH091657) funded by the 16 NIH Institutes and Centers that support the NIH Blueprint for

831 Neuroscience Research; and by the McDonnell Center for Systems Neuroscience at Washington
832 University.

833

834 **Author contributions:** AIL, JV, EAS, SA and MLK conceived the study. AIL, JV, PAMM, SA,
835 MLK and EAS designed the methodology and the analysis. AIL analysed the data. JV, PAMM,
836 MMC, and IP contributed to data analysis. PF, GBW, JA, JDP, RA, DKM, EAS, LR, RLCH were
837 involved in designing the original studies for which the present data were collected. PF, MMC,
838 GBW, JA, EAS, RA, RLCH, LR all participated in data collection. AIL, EAS and SA wrote the
839 manuscript with feedback from all co-authors.

840

841 **Conflicts of interest:** the authors declare that no conflicts of interest exist.

842 **Data and materials availability.** The datasets analysed during the current study can be made
843 available on request. The CONN toolbox is freely available online
844 (<http://www.nitrc.org/projects/conn>). The Java Information Dynamics Toolbox is freely available
845 online: <https://github.com/jlizier/jidt>.

846

847 REFERENCES

848

- 849 1. Northoff, G., Wainio-Theberge, S. & Evers, K. Is temporo-spatial dynamics the common
850 currency of brain and mind? In *Quest of Spatiotemporal Neuroscience*. (2019).
851 doi:10.1016/j.pnrev.2019.05.002
- 852 2. Demertzi, A. *et al.* Human consciousness is supported by dynamic complex patterns of
853 brain signal coordination. *Sci. Adv.* **5**, 1–12 (2019).
- 854 3. Luppi, A. I. *et al.* Consciousness-specific dynamic interactions of brain integration and
855 functional diversity. *Nat. Commun.* (2019).
- 856 4. Cao, B. *et al.* Abnormal dynamic properties of functional connectivity in disorders of
857 consciousness. *NeuroImage Clin.* **24**, (2019).
- 858 5. Lord, L. D. *et al.* Dynamical exploration of the repertoire of brain networks at rest is
859 modulated by psilocybin. *Neuroimage* **199**, 127–142 (2019).
- 860 6. Barttfeld, P. *et al.* Signature of consciousness in the dynamics of resting-state brain
861 activity. *Proc. Natl. Acad. Sci.* **112**, 887–892 (2015).
- 862 7. Varley, T. F. *et al.* Consciousness & Brain Functional Complexity in Propofol
863 Anaesthesia. *Sci. Rep.* **10**, (2020).
- 864 8. Atasoy, S., Deco, G., Krriegelbach, M. & Pearson, J. Harmonic Brain Modes: A Unifying
865 Framework for Linking Space and Time in Brain Dynamic. *Neurosci.* (2018).

866 doi:10.1177/1073858417728032
867 9. Atasoy, S. *et al.* Connectome-harmonic decomposition of human brain activity reveals
868 dynamical repertoire re-organization under LSD. *Sci. Rep.* **7**, 1–18 (2017).
869 10. Atasoy, S., Vohryzek, J., Deco, G., Carhart-harris, R. L. & Kringelbach, M. L. Common
870 neural signatures of psychedelics: Frequency-specific energy changes and repertoire
871 expansion revealed using connectome-harmonic decomposition. **242**, (2018).
872 11. Wang, M. B., Owen, J. P., Mukherjee, P. & Raj, A. Brain network eigenmodes provide a
873 robust and compact representation of the structural connectome in health and disease.
874 *PLoS Comput. Biol.* **13**, (2017).
875 12. Murray, J. D. *Mathematical Biology II - Spatial Models and Biomedical Applications.*
876 *Mathematical Biology II - Spatial Models and Biomedical Applications* (Springer, 2008).
877 doi:10.1007/b98869
878 13. Atasoy, S., Donnelly, I. & Pearson, J. Human brain networks function in connectome-
879 specific harmonic waves. *Nat. Commun.* **7**, (2016).
880 14. Gabay, N. C. & Robinson, P. A. Cortical geometry as a determinant of brain activity
881 eigenmodes: Neural field analysis. *Phys. Rev. E* **96**, 32413 (2017).
882 15. Carhart-Harris, R. L. *et al.* The entropic brain: a theory of conscious states informed by
883 neuroimaging research with psychedelic drugs. *Front. Hum. Neurosci.* **8**, 20 (2014).
884 16. Carhart-Harris, R. L. & Friston, K. J. REBUS and the anarchic brain: Toward a unified
885 model of the brain action of psychedelics. *Pharmacol. Rev.* **71**, 316–344 (2019).
886 17. Schartner, M. M., Carhart-Harris, R. L., Barrett, A. B., Seth, A. K. &
887 Muthukumaraswamy, S. D. Increased spontaneous MEG signal diversity for psychoactive
888 doses of ketamine, LSD and psilocybin. *Sci. Rep.* **7**, 46421 (2017).
889 18. Schartner, M. *et al.* Complexity of multi-dimensional spontaneous EEG decreases during
890 propofol induced general anaesthesia. *PLoS One* **10**, (2015).
891 19. Schartner, M. M. *et al.* Global and local complexity of intracranial EEG decreases during
892 NREM sleep. *Neurosci. Conscious.* (2017). doi:10.1093/nc/niw022
893 20. Sarasso, S. *et al.* Consciousness and Complexity during Unresponsiveness Induced by
894 Propofol, Xenon, and Ketamine. *CURBIO* **25**, 3099–3105 (2015).
895 21. Li, D. & Mashour, G. A. Cortical dynamics during psychedelic and anesthetized states
896 induced by ketamine. *Neuroimage* **196**, 32–40 (2019).
897 22. Bayne, T. & Carter, O. Dimensions of consciousness and the psychedelic state. *Neurosci.*
898 *Conscious.* **2018**, (2018).
899 23. Stamatakis, E. A., Adapa, R. M., Absalom, A. R. & Menon, D. K. Changes in resting
900 neural connectivity during propofol sedation. *PLoS One* **5**, e14224 (2010).
901 24. Brown, E. N., Lydic, R. & Schiff, N. D. General Anesthesia, Sleep, and Coma. *N. Engl. J.*
902 *Med.* **27**, 2638–50 (2010).
903 25. Owen, A. M. *et al.* Detecting awareness in the vegetative state. *Science (80-)* **313**, 1402
904 (2006).
905 26. Monti, M. M. *et al.* Willful modulation of brain activity in disorders of consciousness. *N.*
906 *Engl. J. Med.* **362**, 579–589 (2010).
907 27. Radtke, F. M. *et al.* Risk factors for inadequate emergence after anesthesia: Emergence
908 delirium and hypoactive emergence. *Minerva Anestesiol.* **76**, 394–404 (2010).
909 28. Xará, D., Silva, A., Mendonça, J. & Abelha, F. Inadequate emergence after anesthesia:
910 emergence delirium and hypoactive emergence in the Postanesthesia Care Unit. *J. Clin.*
911 *Anesth.* **25**, 439–446 (2013).

912 29. Dandash, O. *et al.* Selective Augmentation of Striatal Functional Connectivity Following
913 NMDA Receptor Antagonism: Implications for Psychosis. *Neuropsychopharmacology* **40**,
914 622–631 (2015).

915 30. Olney, J. W., Newcomer, J. W. & Farber, N. B. NMDA receptor hypofunction model of
916 schizophrenia. *J. Psychiatr. Res.* **33**, 523–533 (1999).

917 31. Corlett, P. R., Honey, G. D. & Fletcher, P. C. Prediction error, ketamine and psychosis:
918 An updated model. *J. Psychopharmacol.* **30**, 1145–1155 (2016).

919 32. Carhart-Harris, R. L., Brugger, S., Nutt, D. J. & Stone, J. M. Psychiatry's next top model:
920 Cause for a re-think on drug models of psychosis and other psychiatric disorders. *J.*
921 *Psychopharmacol.* **27**, 771–778 (2013).

922 33. Preti, M. G. & Van De Ville, D. Decoupling of brain function from structure reveals
923 regional behavioral specialization in humans. *Nat. Commun.* **10**, (2019).

924 34. Krishnan, A., Williams, L. J., McIntosh, A. R. & Abdi, H. Partial Least Squares (PLS)
925 methods for neuroimaging: A tutorial and review. *Neuroimage* **56**, 455–475 (2011).

926 35. Scott, G. & Carhart-Harris, R. L. Psychedelics as a treatment for disorders of
927 consciousness. *Neurosci. Conscious.* **2019**, niz003 (2019).

928 36. Huang, Z. *et al.* Brain imaging reveals covert consciousness during behavioral
929 unresponsiveness induced by propofol. *Sci. Rep.* **8**, 1–11 (2018).

930 37. Ní Mhuircheartaigh, R., Warnaby, C., Rogers, R., Jbabdi, S. & Tracey, I. Slow-wave
931 activity saturation and thalamocortical isolation during propofol anesthesia in humans. *Sci.*
932 *Transl. Med.* **5**, 208ra148 (2013).

933 38. Leslie, K. *et al.* Dreaming and Electroencephalographic Changes during Anesthesia
934 Maintained with Propofol or Desflurane. *Anesthesiology* **111**, 547–555 (2009).

935 39. Naci, L., Sinai, L. & Owen, A. M. Detecting and interpreting conscious experiences in
936 behaviorally non-responsive patients. *Neuroimage* (2015).
937 doi:10.1016/j.neuroimage.2015.11.059

938 40. Casali, A. G. *et al.* A Theoretically Based Index of Consciousness Independent of Sensory
939 Processing and Behavior. in *Science translational medicine* **5**, 1–10 (2013).

940 41. Corlett, P. R. *et al.* Frontal responses during learning predict vulnerability to the
941 psychotogenic effects of ketamine: Linking cognition, brain activity, and psychosis. *Arch.*
942 *Gen. Psychiatry* **63**, 611–621 (2006).

943 42. Whitfield-Gabrieli, S. & Nieto-Castanon, A. Conn: A Functional Connectivity Toolbox
944 for Correlated and Anticorrelated Brain Networks. *Brain Connect.* **2**, 125–141 (2012).

945 43. Behzadi Y, Restom K, Liau J & Liu TT. A component based noise correction method
946 (CompCor) for BOLD and perfusion based fMRI. *Neuroimage* **37**, 90–101 (2007).

947 44. Bruno, M.-A., Vanhaudenhuyse, A., Thibaut, A., Moonen, G. & Laureys, S. From
948 unresponsive wakefulness to minimally conscious PLUS and functional locked-in
949 syndromes: recent advances in our understanding of disorders of consciousness. *J. Neurol.*
950 **258**, 1373–1384 (2011).

951 45. Wannez, S. *et al.* Prevalence of coma-recovery scale-revised signs of consciousness in
952 patients in minimally conscious state. *Neuropsychol. Rehabil.* **28**, 1350–1359 (2018).

953 46. Fernández-Espejo, D., Norton, L. & Owen, A. M. The clinical utility of fMRI for
954 identifying covert awareness in the vegetative state: A comparison of sensitivity between
955 3T and 1.5T. *PLoS One* **9**, (2014).

956 47. Carhart-Harris, R. L. *et al.* Neural correlates of the LSD experience revealed by
957 multimodal neuroimaging. *Proc. Natl. Acad. Sci.* **113**, 201518377 (2016).

958 48. Chung, F. *Spectral Graph Theory*. (American Mathematical Society, 1997).

959 49. Chuen Lee, L., Liong, C.-Y. & Aziz Jemain, A. Partial least squares-discriminant analysis
960 (PLS-DA) for classification of high-dimensional (HD) data: a review of contemporary
961 practice strategies and knowledge gaps †. *Analyst* **143**, 3526 (2018).

962 50. Lizier, J. T. JIDT: An Information-Theoretic Toolkit for Studying the Dynamics of
963 Complex Systems. *Front. Robot. AI* **1**, 1–37 (2014).

964 51. Cover, T. M. & Thomas, J. A. *Elements of Information Theory. Elements of Information*
965 *Theory* (Wiley-Interscience, 2005). doi:10.1002/047174882X

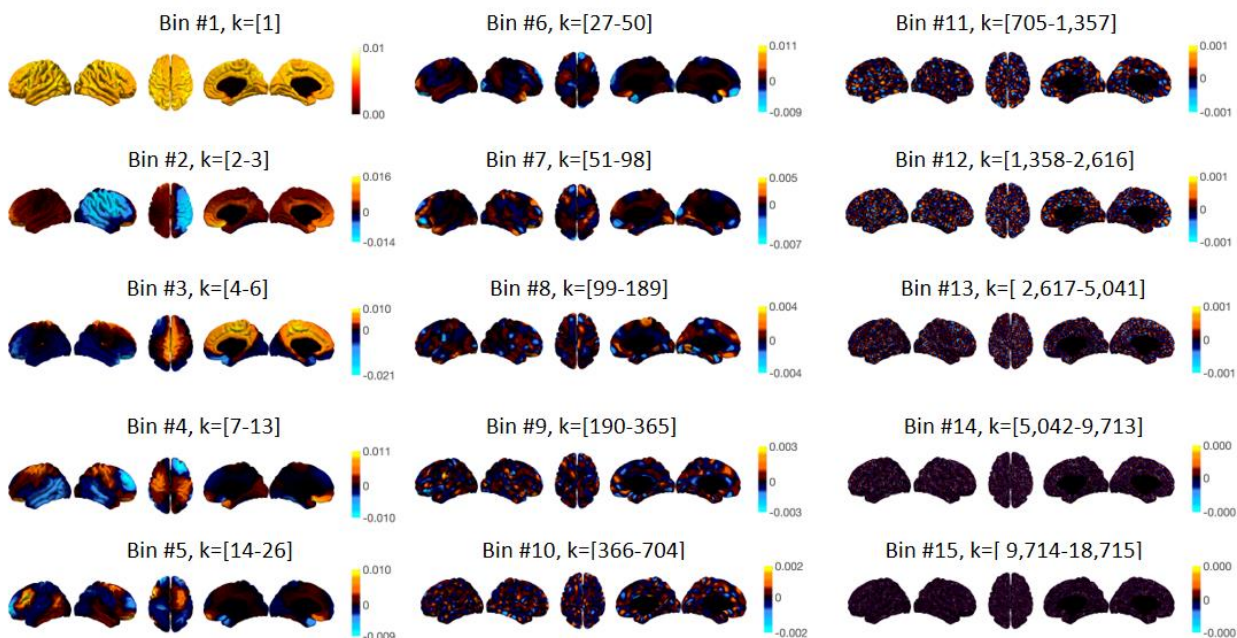
966 52. Benjamini, Y. & Hochberg, Y. Controlling the False Discovery Rate: A Practical and
967 Powerful Approach to Multiple Testing. *J. R. Stat. Soc. Ser. B* **57**, 289–300 (1995).

Supplementary Information for:

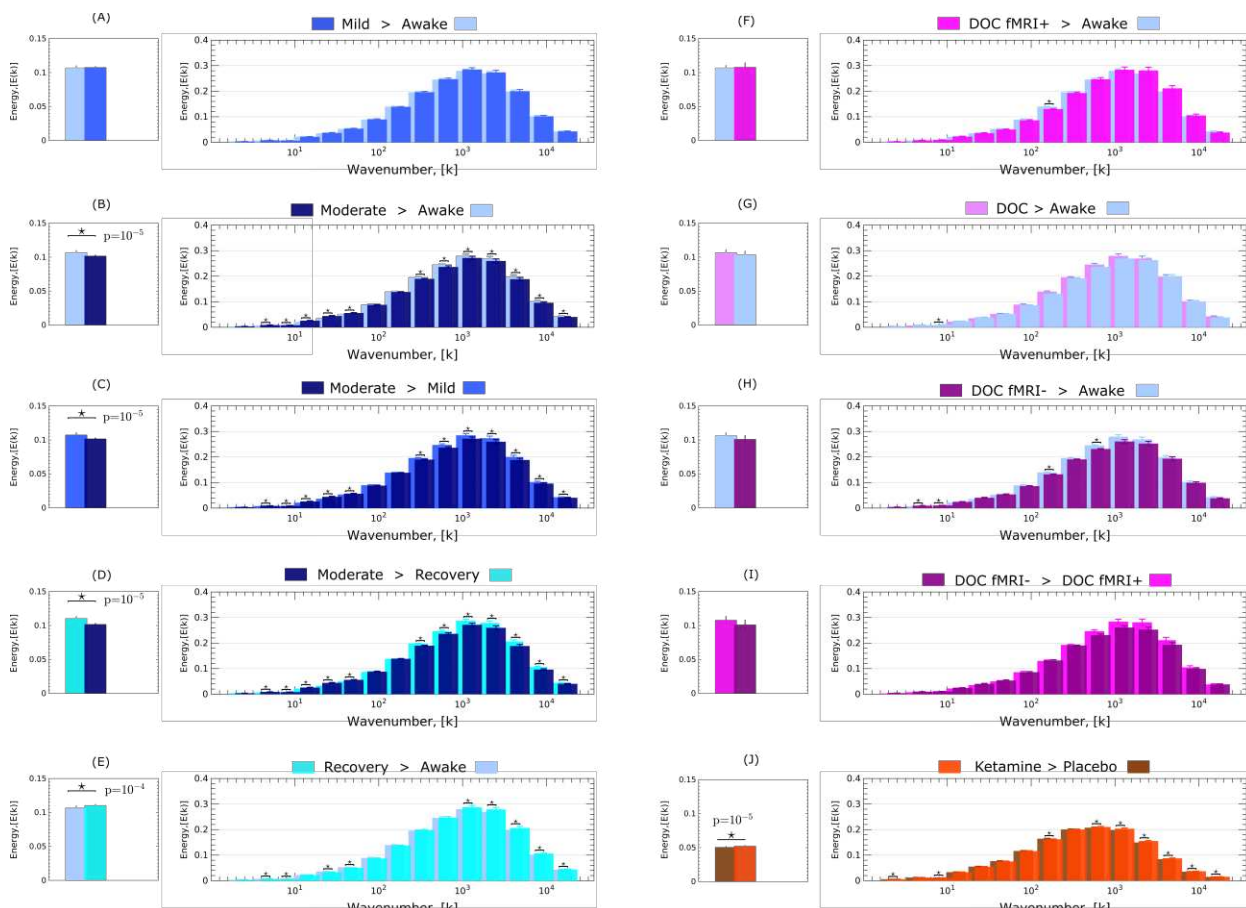
Connectome Harmonic Decomposition of Human Brain Dynamics Reveals a Landscape of Consciousness

Luppi A.I. ^{a,b,*}, Vohryzek J. ^{c,d}, Kringelbach M. L. ^{c,d}, Mediano P.A.M. ^e, Craig M. M. ^{a,b}, Adapa R. ^a, Carhart-Harris, R. L. ^f, Roseman, L. ^f, Pappas I. ^{a,b,g}, Finioia P. ^{a,h}, Williams G. B. ^{b,i}, Allanson J. ^{b,j}, Pickard J. D. ^{b,h,i}, Menon D. K. ^a, Atasoy S. ^{c,d}, & Stamatakis E.A. ^{a,b}

Supplementary Figures



Supplementary Figure 1. Binned connectome harmonics. Surface projections of connectome harmonics averaged over each of 15 logarithmically spaced bins (with corresponding wavenumbers k indicated in braces), showing the progressive increase in complexity and granularity of the connectome harmonic patterns, with increasing spatial frequency.



19

20

21

22

23

24

25

26

27

28

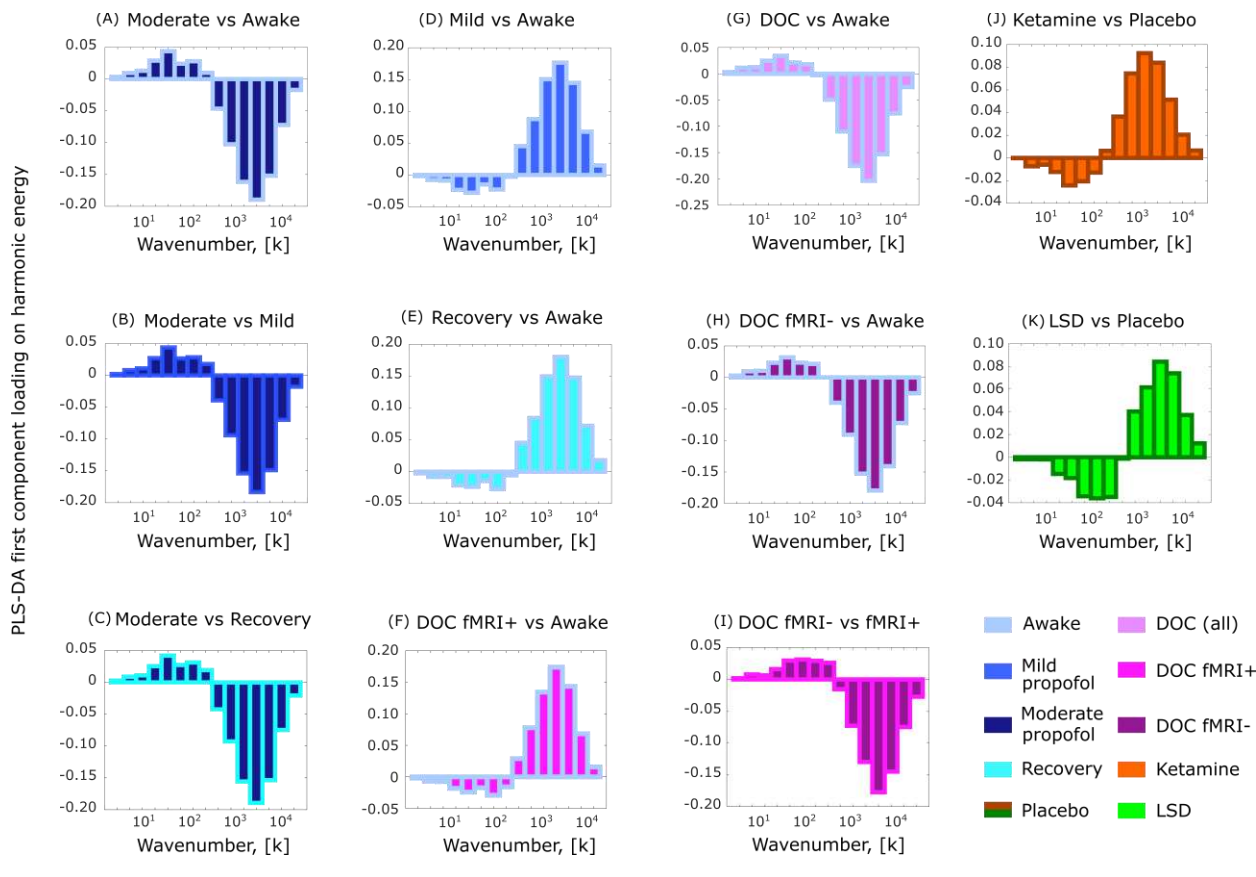
29

30

31

32

33

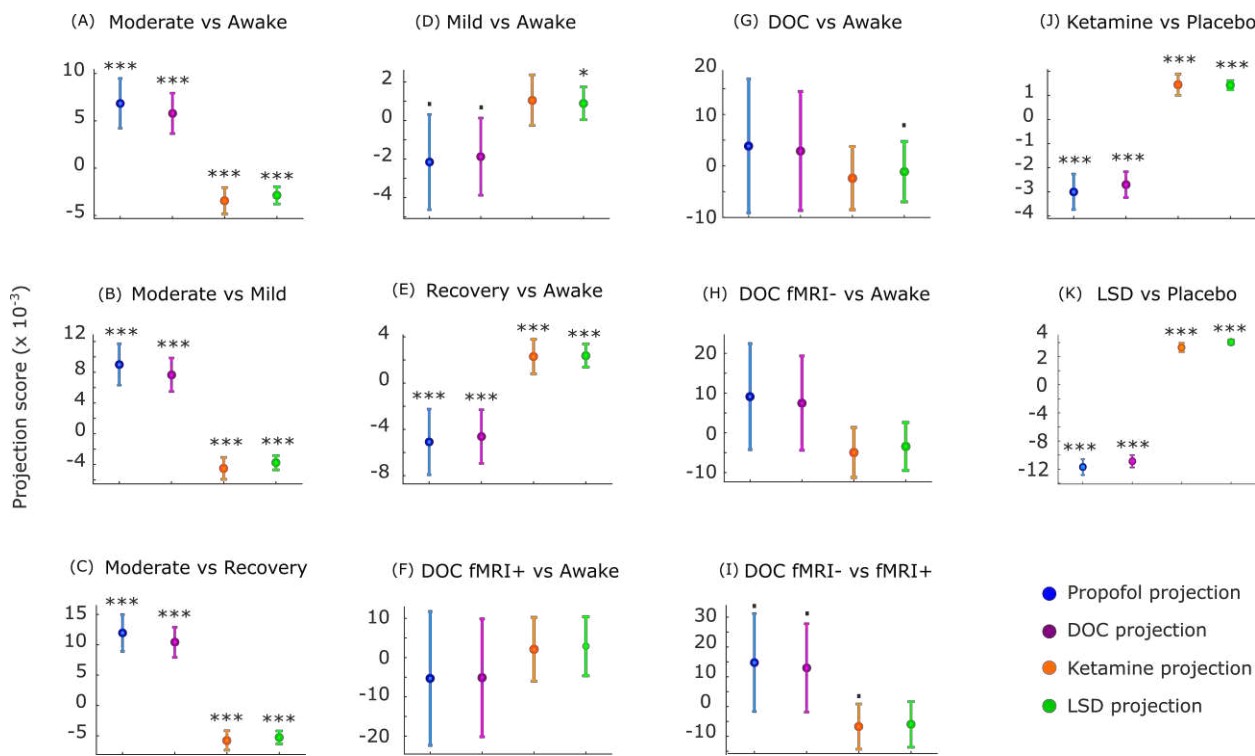


34

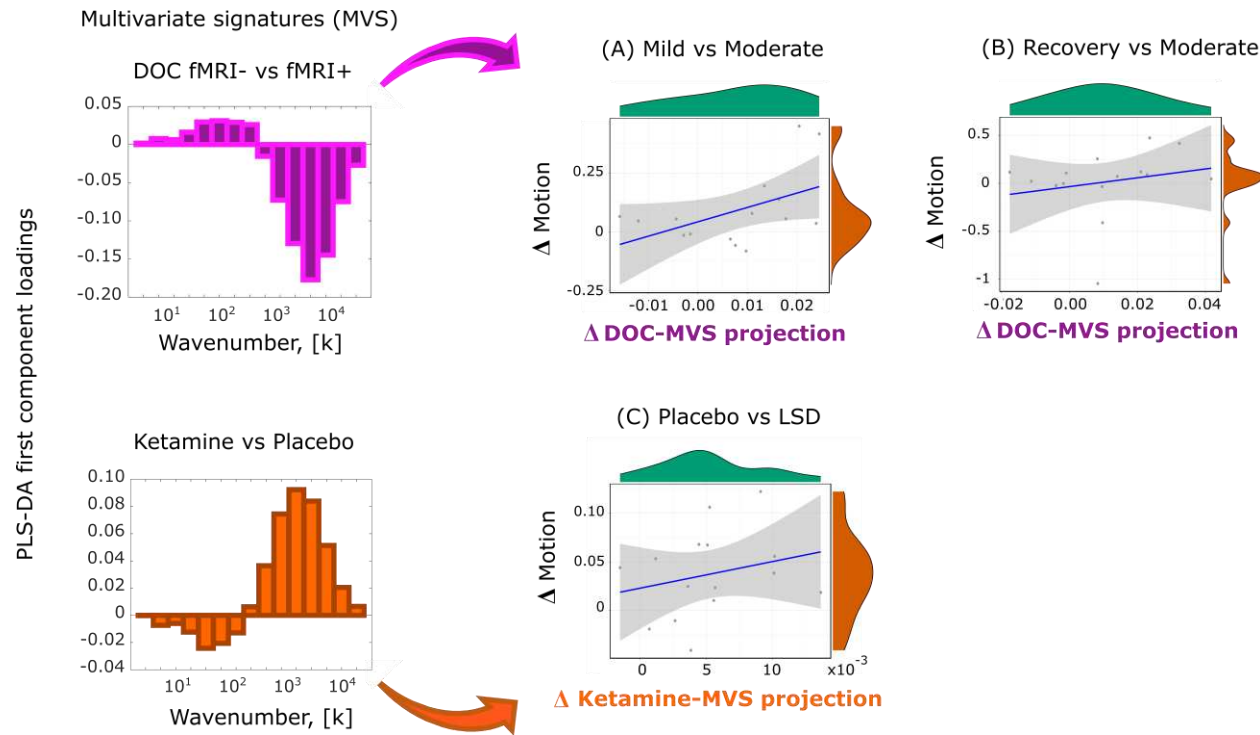
35 **Supplementary Figure 3. Similarity of PLS-DA maximally discriminative components of connectome harmonic**
36 **energy between states of consciousness.** (a) Moderate anaesthesia > wakefulness. (b) Moderate anaesthesia > mild
37 sedation. (c) Moderate anaesthesia > post-anaesthetic recovery. (d) Mild sedation > wakefulness. (e) Post-anaesthetic
38 recovery > wakefulness. (f) DOC fMRI+ patients > awake healthy controls. (g) DOC patients > awake healthy
39 controls. (h) DOC fMRI- patients > awake healthy controls. (i) fMRI- > fMRI+ DOC patients. (j) Ketamine > placebo.
40 (k) LSD > placebo. Bar colour indicates the target state; contours indicate the reference state.

41

42



Supplementary Figure 4. Maximally discriminative patterns of connectome harmonic energy are generalisable across states of consciousness. Each panel shows the fixed effects (and 95% CI) of contrasting the projections (dot product) of MDC patterns from four source states (moderate propofol anaesthesia, DOC patients, ketamine and LSD) onto each pair of the states of consciousness under comparison. (a) Moderate anaesthesia > wakefulness. (b) Moderate anaesthesia > mild sedation. (c) Moderate anaesthesia > post-anaesthetic recovery. (d) Mild sedation > wakefulness. (e) Post-anaesthetic recovery > wakefulness. (f) DOC fMRI+ patients > awake healthy controls. (g) DOC patients > awake healthy controls. (h) DOC fMRI- patients > awake healthy controls. (i) fMRI- > fMRI+ DOC patients. (j) Ketamine > placebo. (k) LSD > placebo. * $p < 0.05$; ** $p < 0.01$; *** $p < 0.001$; . $p < 0.10$.



56

57

58 **Supplementary Figure 5. Change in projection onto cross-dataset multivariate energy signature (MVS) does**
59 **not significantly correlate with differences in subject motion in the scanner.** (a) Scatterplot of delta in connectome
60 harmonic energy projection onto the MVS derived from the DOC dataset, versus the delta in head motion (moderate
61 anaesthesia minus mild anaesthesia). (b) Scatterplot of delta in connectome harmonic energy projection onto the MVS
62 derived from the DOC dataset, versus the delta in head motion (moderate anaesthesia minus recovery). (c) Scatterplot
63 of delta in connectome harmonic energy projection onto the MVS derived from the ketamine dataset, versus the delta
64 in head motion (LSD minus placebo).

65

66

67

68

69

70

71

72

73

74 **Supplementary Tables**

75

76 **Supplementary Table 1.** LME results for total connectome harmonic energy (units are $\times 10^{-3}$). * $p < 0.05$; ** $p < 0.01$;
77 *** $p < 0.001$; . $p < 0.10$; n.s. not significant.

78

Contrast	Fixed Effect	95% CI Lower	95% CI Upper	p-value	Significance
Awake vs fMRI-	-5.598	-15.603	4.406	0.273	n.s.
fMRI+ vs fMRI-	-6.835	-19.879	6.209	0.304	n.s.
Awake vs DOC	-3.113	-12.533	6.307	0.517	n.s.
Awake vs Moderate Propofol	-4.943	-6.593	-3.293	$p < 0.001$	***
Mild vs Moderate Propofol	-5.724	-7.394	-4.055	$p < 0.001$	***
Recovery vs Moderate Propofol	-8.665	-10.597	-6.733	$p < 0.001$	***
Awake vs fMRI+	1.236	-10.359	12.832	0.834	n.s.
Awake vs Mild Propofol	0.782	-0.758	2.321	0.320	n.s.
Awake vs Recovery	3.722	1.904	5.541	$p < 0.001$	***
Placebo vs Ketamine	1.798	1.425	2.172	$p < 0.001$	***
Placebo vs LSD	8.101	7.472	8.730	$p < 0.001$	***

79

80

81 **Supplementary Table 2.** LME results for the projection onto the PLS-DA first component of different states of
82 consciousness (units are $\times 10^{-3}$). * $p < 0.05$; ** $p < 0.01$; *** $p < 0.001$; . $p < 0.10$; n.s. not significant.

83

Dataset	Source	Fixed Effect	95% CI Lower	95% CI Upper	p-value	Significance
Placebo vs LSD	propofol	-11.71	-12.84	-10.59	p < 0.001	***
	DOC	-10.88	-11.75	-10.01	p < 0.001	***
	ketamine	5.30	4.67	5.93	p < 0.001	***
	LSD	6.08	5.74	6.42	p < 0.001	***
Placebo vs Ketamine	propofol	-3.00	-3.74	-2.26	p < 0.001	***
	DOC	-2.70	-3.24	-2.16	p < 0.001	***
	ketamine	1.44	1.01	1.88	p < 0.001	***
	LSD	1.42	1.23	1.61	p < 0.001	***
Propofol Awake vs Mild	propofol	-2.16	-4.62	0.31	0.087	.
	DOC	-1.88	-3.88	0.13	0.067	.
	ketamine	1.06	-0.26	2.37	0.115	
	LSD	0.89	0.04	1.75	0.040	*
Propofol Awake vs Recovery	propofol	-5.08	-7.92	-2.25	p < 0.001	***
	DOC	-4.62	-6.94	-2.30	p < 0.001	***
	ketamine	2.30	0.80	3.79	0.003	**
	LSD	2.38	1.38	3.38	p < 0.001	***
Propofol Awake vs Moderate	propofol	6.85	4.23	9.48	p < 0.001	***
	DOC	5.79	3.66	7.93	p < 0.001	***
	ketamine	-3.45	-4.84	-2.06	p < 0.001	***
	LSD	-2.88	-3.79	-1.97	p < 0.001	***
Propofol Mild vs Moderate	propofol	9.01	6.33	11.69	p < 0.001	***

	DOC	7.67	5.49	9.85	p < 0.001	***
	ketamine	-4.51	-5.93	-3.08	p < 0.001	***
	LSD	-3.78	-4.70	-2.85	p < 0.001	***
Propofol Recovery vs Moderate	propofol	11.94	8.90	14.97	p < 0.001	***
	DOC	10.41	7.93	12.90	p < 0.001	***
	ketamine	-5.75	-7.34	-4.15	p < 0.001	***
	LSD	-5.26	-6.33	-4.19	p < 0.001	***
DOC fMRI+ vs fMRI-	propofol	14.43	-1.97	30.83	0.085	.
	DOC	12.65	-2.18	27.48	0.094	.
	ketamine	-7.04	-14.63	0.55	0.069	.
	LSD	-6.32	-13.97	1.33	0.105	.
Awake vs DOC	propofol	3.87	-9.13	16.86	0.098	.
	DOC	2.90	-8.67	14.46	0.101	n.s.
	ketamine	-2.38	-8.52	3.77	0.105	n.s.
	LSD	-1.13	-7.00	4.74	0.109	n.s.
Awake vs DOC fMRI+	propofol	-5.31	-22.34	11.72	0.112	n.s.
	DOC	-5.16	-20.17	9.85	0.116	n.s.
	ketamine	2.11	-6.02	10.23	0.120	n.s.
	LSD	2.89	-4.64	10.42	0.123	n.s.
Awake vs DOC fMRI-	propofol	9.11	-4.20	22.43	0.127	n.s.
	DOC	7.50	-4.37	19.36	0.131	n.s.
	ketamine	-4.94	-11.21	1.34	0.134	n.s.
	LSD	-3.43	-9.46	2.60	0.138	n.s.

84
85
86
87

88 **Supplementary Table 3.** Correlations of cross-dataset projections onto MDCs with mean motion difference. $p < 0.10$;
 89 n.s. not significant.
 90

		Spearman's ρ	CI 95%	p-value	Sig
	Moderate-Mild Motion Delta vs DOC Projection Delta	0.45	[-0.08; 0.78]	0.089	.
	Moderate-Recovery Motion Delta vs DOC Projection Delta	0.31	[-0.24; 0.71]	0.254	n.s.
	LSD-Placebo Motion Delta vs Ketamine Projection Delta	0.24	[-0.31; 0.67]	0.383	n.s.

91
 92
 93 **Supplementary Table 4.** LME results for repertoire diversity of the connectome harmonics. * $p < 0.05$; ** $p < 0.01$;
 94 *** $p < 0.001$; ** $p < 0.01$; . $p < 0.10$; n.s. not significant.
 95

Contrast	Fixed Effect	95% CI Lower	95% CI Upper	p-value	Significance
Awake vs fMRI-	-0.074	-0.129	-0.018	0.009	**
fMRI+ vs fMRI-	-0.063	-0.133	0.007	0.079	.
Awake vs DOC	-0.051	-0.102	0.000	0.051	.
Awake vs Moderate Propofol	-0.039	-0.052	-0.026	$p < 0.001$	***
Mild vs Moderate Propofol	-0.040	-0.054	-0.027	$p < 0.001$	***
Recovery vs Moderate Propofol	-0.040	-0.055	-0.025	$p < 0.001$	***
Awake vs fMRI+	-0.011	-0.064	0.042	0.691	n.s.
Awake vs Mild Propofol	0.001	-0.011	0.013	0.880	n.s.
Awake vs Recovery	0.001	-0.013	0.014	0.928	n.s.
Placebo vs Ketamine	0.020	0.016	0.024	$p < 0.001$	***
Placebo vs LSD	0.054	0.049	0.059	$p < 0.001$	***

96
 97
 98